Article

Cell Reports

# The Myb-MuvB Complex Is Required for YAP-Dependent Transcription of Mitotic Genes

## Graphical Abstract

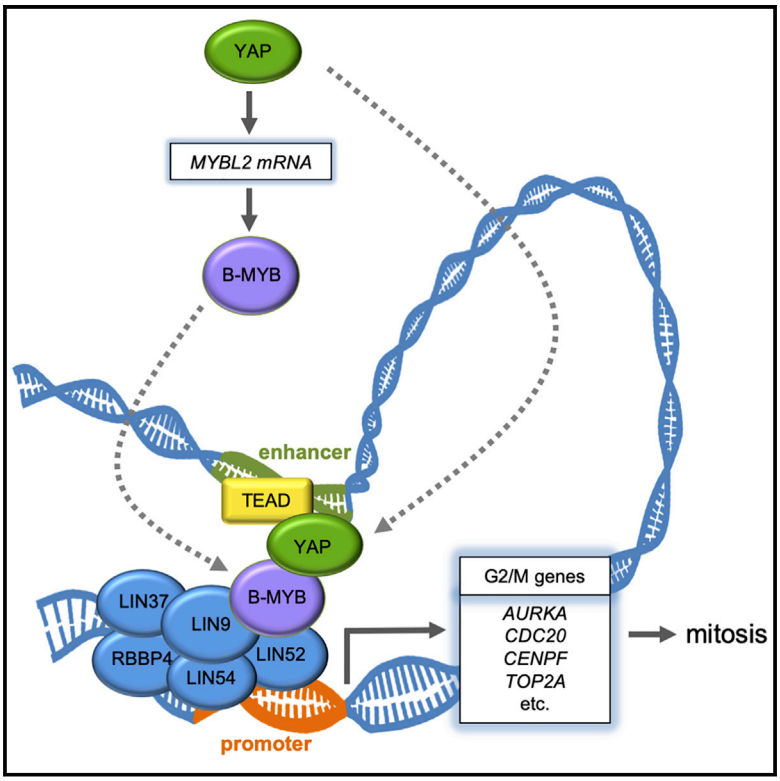


## Authors

Grit Pattschull, Susanne Walz, Marco Gründl, ..., Andreas Rosenwald, Björn von Eyss, Stefan Gaubatz

## Correspondence

stefan.gaubatz@biozentrum.uni-wuerzburg.de

## In Brief

YAP and TAZ, downstream effectors of the Hippo pathway, are important regulators of proliferation. Here, Pattschull et al. show that YAP induces the expression of the MMB subunit B-MYB and promotes the binding of B-MYB to the promoters of G2/M genes from distant enhancers, leading to the enhanced expression of mitotic genes.

## Highlights

- YAP induces the expression and chromatin binding of the Myb-MuvB subunit B-MYB
- YAP interacts with B-MYB-regulated promoters from distant enhancers
- B-MYB is required for YAP-mediated expression of mitotic genes
- The cooperation between YAP and B-MYB is critical for YAP-mediated entry into mitosis

Pattschull et al., 2019, Cell Reports *27*, 3533–3546
June 18, 2019 
https://doi.org/10.1016/j.celrep.2019.05.071

CellPress

Cell Reports
Article



# The Myb-MuvB Complex Is Required for YAP-Dependent Transcription of Mitotic Genes

Grit Pattschull,[1] Susanne Walz,[2] Marco Gründl,[1] Melissa Schwab,[1] Eva Rühl,[1] Apoorva Baluapuri,[3] Anita Cindric-Vranesic,[5] Susanne Kneitz,[1] Elmar Wolf,[3] Carsten P. Ade,[1] Andreas Rosenwald,[4] Björn von Eyss,[5] and Stefan Gaubatz[1,6,*]

[1]Theodor Boveri Institute and Comprehensive Cancer Center Mainfranken, Biocenter, University of Wuerzburg, Wuerzburg 97074, Germany
[2]Comprehensive Cancer Center Mainfranken, Core Unit Bioinformatics, Biocenter, University of Wuerzburg, Wuerzburg 97074, Germany
[3]Cancer Systems Biology Group, Biochemistry and Molecular Biology, University of Wuerzburg, Wuerzburg 97074, Germany
[4]Institute of Pathology and Comprehensive Cancer Center Mainfranken, University of Wuerzburg, Wuerzburg 97080, Germany
[5]Leibniz Institute on Aging, Fritz Lipmann Institute e.V., Jena 07745, Germany
[6]Lead Contact
*Correspondence: stefan.gaubatz@biozentrum.uni-wuerzburg.de
https://doi.org/10.1016/j.celrep.2019.05.071

## SUMMARY

**YAP and TAZ, downstream effectors of the Hippo pathway, are important regulators of proliferation. Here, we show that the ability of YAP to activate mitotic gene expression is dependent on the Myb-MuvB (MMB) complex, a master regulator of genes expressed in the G2/M phase of the cell cycle. By carrying out genome-wide expression and binding analyses, we found that YAP promotes binding of the MMB subunit B-MYB to the promoters of mitotic target genes. YAP binds to B-MYB and stimulates B-MYB chromatin association through distal enhancer elements that interact with MMB-regulated promoters through chromatin looping. The cooperation between YAP and B-MYB is critical for YAP-mediated entry into mitosis. Furthermore, the expression of genes coactivated by YAP and B-MYB is associated with poor survival of cancer patients. Our findings provide a molecular mechanism by which YAP and MMB regulate mitotic gene expression and suggest a link between two cancer-relevant signaling pathways.**

## INTRODUCTION

YAP and the related TAZ protein are transcriptional coactivators that act downstream of the Hippo signaling pathway, a highly conserved signaling pathway that controls organ size and cell proliferation (Hong and Guan, 2012). The Hippo signaling cascade consists of the core kinases MST1, MST2, LATS1, and LATS2, and their regulatory subunits Salvador (SAV1) and MOB1 (Meng et al., 2016). LATS kinases phosphorylate YAP and TAZ, resulting in their nuclear exclusion and degradation via the proteasome. When Hippo activity is low, YAP and TAZ translocate into the nucleus and promote transcription together with transcription factors of the TEAD family. YAP potently induces proliferation and leads to abnormal cell growth and tumorigenesis in many human cancers, making it a potential target for anti-cancer therapy.

It has been noted that the transcriptional response to YAP and TAZ is similar to the transcriptional program induced by E2F transcription factors, which, like YAP, also induce the G1 to S transition during the cell cycle (Ehmer et al., 2014; Kapoor et al., 2014; Zanconato et al., 2015). Furthermore, YAP and E2F synergize to induce DNA-replication genes and promote proliferation (Kapoor et al., 2014). Although co-binding of YAP and E2F to promoters of common target genes has been observed, more recent data indicate that YAP regulates genes mainly from distant enhancers (Galli et al., 2015; Stein et al., 2015; Zanconato et al., 2015). This suggests that YAP could cooperate with E2F factors at promoters through chromatin looping, a model that has yet to be tested.

YAP not only activates G1/S genes but also genes that are required for mitosis and cytokinesis (Bai et al., 2012; Lange et al., 2015; Tremblay et al., 2014; Zanconato et al., 2015). However, thus far no mechanism for the regulation of G2/M genes by YAP is known. Cooperation of YAP with E2F to activate these genes is unlikely as G2/M genes generally lack E2F promoter elements. However, it is known that G2/M genes are activated by MuvB complexes together with the B-MYB transcription factor (Fischer and Müller, 2017), raising the possibility that YAP cooperates with MuvB to induce mitotic genes. MuvB is an evolutionary conserved multisubunit complex that regulates the expression of cell-cycle genes (Sadasivam and DeCaprio, 2013). MuvB, consisting of the five proteins LIN9, LIN37, LIN52, LIN54, and RBBP4, associates with the p130 retinoblastoma protein paralog and with E2F4 and DP1 to form DREAM, which represses cell-cycle genes in quiescence and early G1 (Litovchick et al., 2007; Schmit et al., 2007). In contrast, in S phase, the interaction of the MuvB core with p130, E2F4, and DP1 is lost and MuvB binds to the B-MYB (MYBL2) transcription factor to form the Myb-MuvB (MMB) complex (Schmit et al., 2007; Osterloh et al., 2007; Pilkinton et al., 2007; Sadasivam et al., 2012). MMB acts to activate the expression of genes whose products have important functions in mitosis and cytokinesis (Reichert et al., 2010; Sadasivam et al., 2012). The functional importance of mitotic gene regulation by MMB is underlined by the observation that the inactivation of MMB in cell lines results in mitotic defects and G2/M arrest (Osterloh et al., 2007; Reichert et al., 2010).

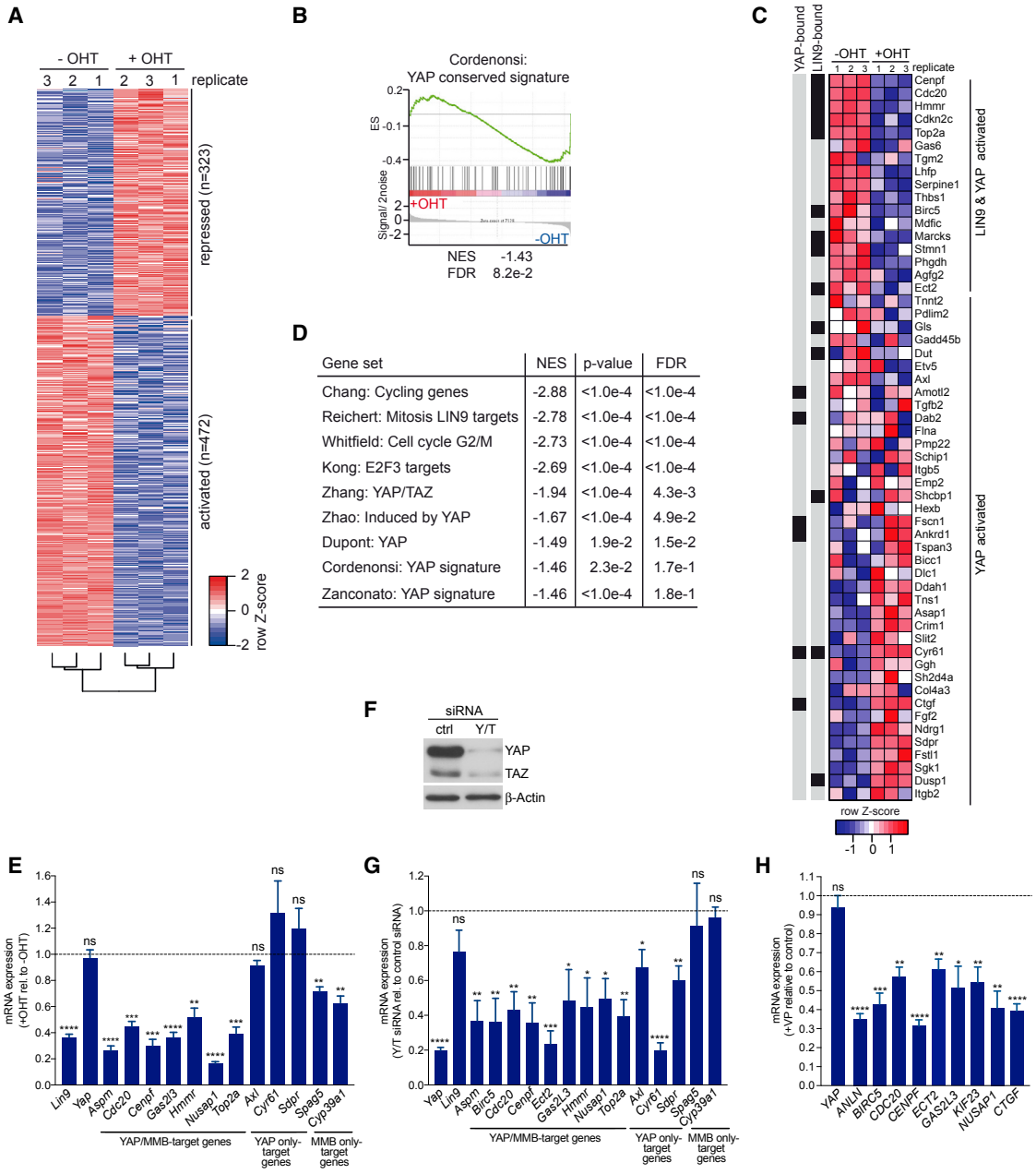


**Figure 1. MMB and YAP Regulate an Overlapping Set of Genes**

(A) Lung adenocarcinoma cells with a conditional allele of the MMB subunit *Lin9* and expressing a hormone-inducible CreER recombinase (KPL-CreER cells) were treated with 4-OHT to delete *Lin9*. RNA was isolated and subjected to RNA-seq. Heatmap of differentially expressed genes after deletion of *Lin9* in KPL cells. Red and blue indicate high and low mRNA expression, respectively.

(B) GSEA of RNA-seq data using the C6 oncogenic gene sets from MSigDB reveals that the conserved YAP-target genes described by Cordenonsi et al. (2011) are downregulated upon the deletion of *Lin9*.

(C) Heatmap depicting the expression of conserved Cordenonsi YAP-signature genes in control cells and *Lin9*-deleted cells. Red and blue indicate high and low mRNA expression, respectively. Black boxes on the left indicate the binding of LIN9 or YAP within 1 kb of the TSS of the corresponding gene as determined by ChIP-seq.

(D) GSEA analysis of the C2 curated gene sets spiked with several previously published YAP-regulated gene sets. NES, normalized enrichment score; FDR, false discovery rate.

(E) The expression of the indicated genes relative to *Hprt* upon deletion of *Lin9* in KPL cells was analyzed by RT-qPCR.

(F) KPL-CreER cells were transfected with a control siRNA or a mixture of siRNAs directed at *Yap* and *Taz*. Depletion of YAP and TAZ was verified by immunoblotting. β-Actin was used as a loading control.

(G) Expression of the indicated genes relative to *Hprt* after siRNA-mediated depletion of *Yap* and *Taz* in KPL-CreER cells was analyzed by RT-qPCR.

*(legend continued on next page)*

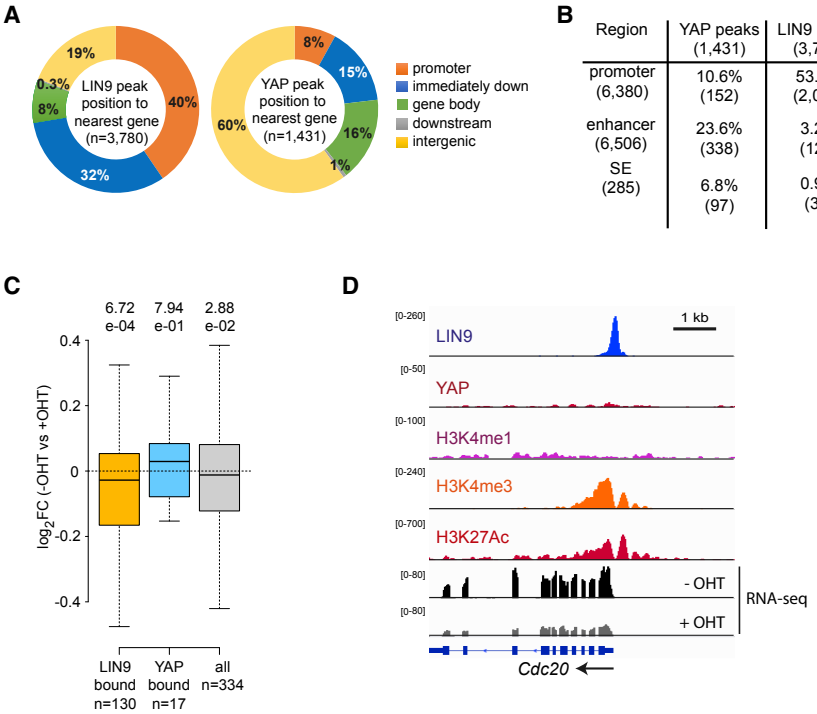


**Figure 2. YAP-Regulated Genes Are Direct Targets of MMB**

(A) Localization of LIN9 and YAP peaks relative to annotated genes as determined by ChIP-seq of KPL-CreER cells.

(B) Percentage of YAP or LIN9 peaks overlapping with active promoters, enhancers, or super-enhancers (SE), as defined by ChIP-seq of histone modifications. Numbers in brackets refer to the number of peaks or regions.

(C) Boxplot showing the $\log_2$ fold expression changes of YAP-target genes described by Zanconato et al. (2015) between control and 4-OHT treated KPL-CreER cells separated into all genes, genes bound by LIN9, and genes bound by YAP in a distance of ±2 kb to the TSS. A total of 334 genes of the signature was present in the RNA-seq analysis. Outliers are not shown. p values were calculated with a two-tailed one-sample Wilcoxon signed-rank test, with $\mu = 0$.

(D) Genome browser tracks at the *Cdc20* locus illustrating the chromatin binding of the indicated proteins. Note that LIN9 but not YAP binds to the promoter of *Cdc20*.

See also Figure S2 and Table S1.

Hippo signaling has previously been linked to the DREAM complex, but not to the MMB complex (Litovchick et al., 2011; Tschöp et al., 2011). Specifically, it has been shown that LATS2 phosphorylates and activates the kinase DYRK1A, which in turn phosphorylates the LIN52 subunit of MuvB. Phosphorylation of LIN52 promotes the assembly of the repressive DREAM complex. Ultimately, this leads to the inhibition of E2F-regulated genes such as *CDC6* and *CDC25A*, resulting in cell-cycle exit and cellular senescence, thus contributing to tumor suppression.

Using transcriptome profiling, we identified an overlap between MMB-dependent genes and evolutionary conserved signatures of genes regulated by YAP. We found that the ability of YAP to activate mitotic gene expression and to promote entry into mitosis is strongly dependent on MMB. Genome-wide DNA-binding analyses showed that MMB binds to a subset of YAP-regulated promoters with functions in mitosis. Functionally, YAP stimulates the chromatin association of B-MYB to MuvB-bound loci from distal enhancers through chromatin looping.

## RESULTS

### MMB and YAP Co-regulate a Set of Genes with Functions in Mitosis

To better understand how MMB contributes to cell-cycle regulation and gene expression in cancer cells, we used murine lung adenocarcinoma KPL cells containing a conditional allele of *Lin9*, a core subunit of MuvB (Iltzsche et al., 2017). We stably expressed a hormone-inducible CreER-recombinase in KPL cells to generate KPL-CreER cells. The addition of 4-hydroxytamoxifen (4-OHT) led to the deletion of *Lin9* and resulted in the differential regulation of several hundred genes (Figures 1A, S1A, and S1B). Using gene set enrichment analysis (GSEA), we observed a previously unknown and significant overlap of LIN9-dependent genes with an evolutionary conserved signature of YAP-regulated genes described by Cordenonsi et al. (2011) (Figures 1B and 1C). In particular, 17 of 56 (30%) conserved YAP-target genes were also regulated by LIN9. Moreover, we detected LIN9-dependent gene expression changes in additional YAP and TAZ-target gene signatures (Dupont et al., 2011; Zanconato et al., 2015; Zhang et al., 2009; Zhao et al., 2008) (Figure 1D).

YAP and the related TAZ protein are transcriptional coactivators that act downstream of the Hippo pathway (Hong and Guan, 2012). Using RT-qPCR, we validated that a subset of known YAP-target genes is dependent on LIN9 in KPL-CreER cells (Figure 1E). In contrast, other YAP-target genes such as *Axl* and *Cyr61* with no direct function in mitosis did not show a significant change in expression after the deletion of *Lin9* ("YAP-only genes"). The depletion of B-MYB also downregulated YAP-target genes, suggesting that these genes are targets of MMB (Figure S1C). Small interfering RNA (siRNA)-mediated knock down of *Yap* and *Taz* with a strong reduction in YAP and TAZ protein levels (Figure 1F) also significantly decreased the

(H) Human lung adenocarcinoma cells were treated with 7.5 μM verteporfin for 24 h, and expression of the indicated MMB-target genes relative to *TBP* was analyzed by RT-qPCR.

(E), (G) and (H) n = 3 biological replicates. Error bars, SEMs. Student's t test. *p < 0.05; **p < 0.01; ***p < 0.001; ****p < 0.0001; ns, not significant, p > 0.05.

See also Figure S1.

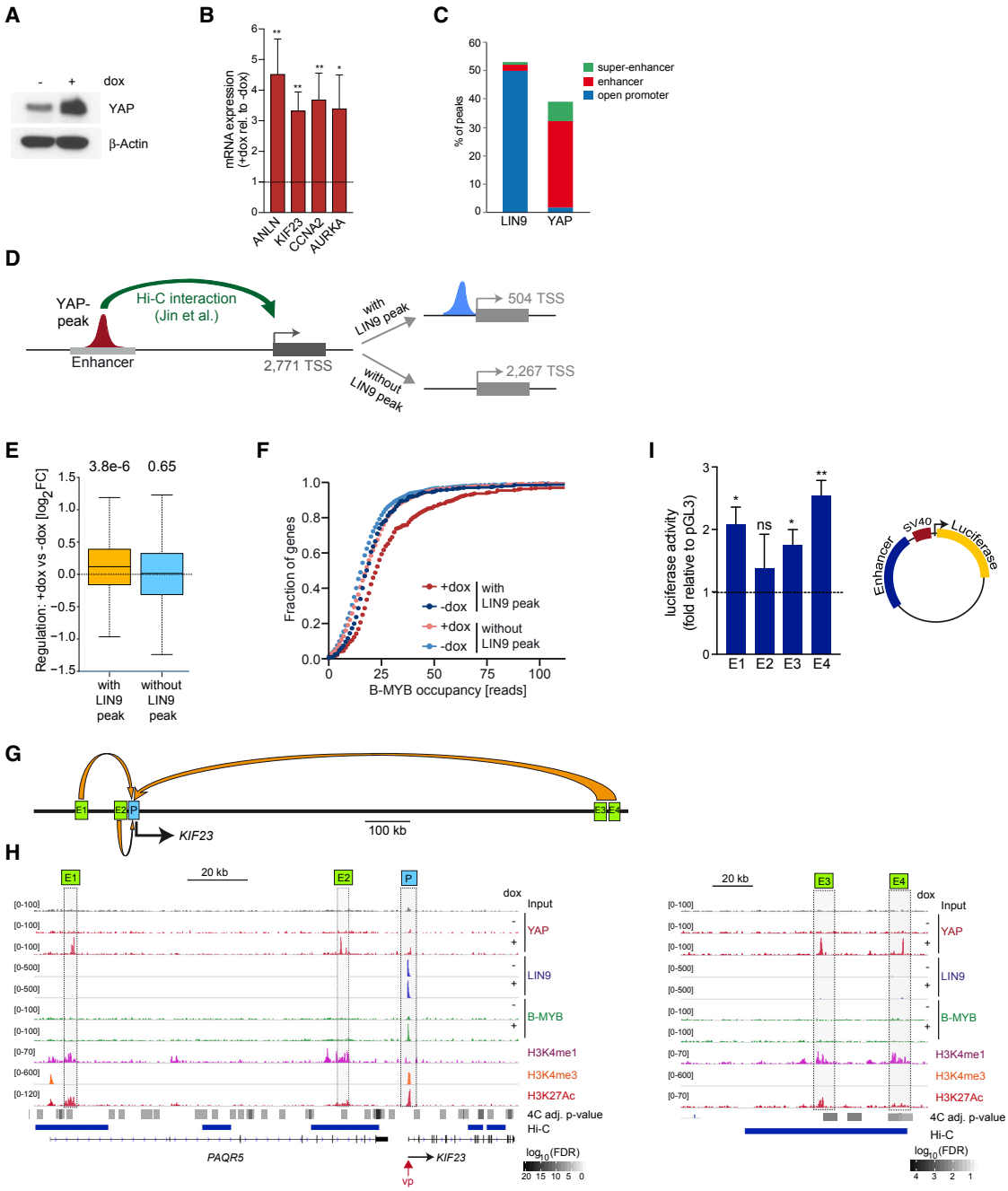


**Figure 3. YAP Activates MMB-Target Genes in MCF10A Cells and Interacts with Their Promoters from Distant Enhancers**

(A) MCF10A cells expressing doxycycline-inducible YAP5SA were treated with and without doxycycline. YAP expression was analyzed by immunoblotting. β-Actin served as a control.

(B) MCF10A-YAP5SA cells were treated as in (A). The expression of the indicated genes relative to *TBP* was analyzed by RT-qPCR. Means and SDs of three biological replicates.

(C) Percentage of LIN9 and YAP peaks located to the indicated genomic regions as determined by ChIP-seq for H3K4me1, H3K4me3, and H3K27Ac.

(D) Strategy to identify YAP-bound enhancers that are linked to LIN9-bound promoters. Enhancers were assigned to promoters using a high-resolution chromatin interaction map (Hi-C) of human IMR90 cells (Jin et al., 2013). Using ChIP-seq with YAP antibodies, we identified a subset of 5,018 enhancers with YAP binding, which were assigned to 2,771 unique TSSs. ChIP-seq with LIN9 antibodies identified 504 LIN9-bound promoters that are linked to YAP-bound enhancers.

(E) Boxplot showing YAP-dependent gene expression changes of genes with (n = 460) or without (n = 1,950) LIN9 peaks that loop to YAP-bound enhancers. p values for the difference of the median to 0 are indicated. Outliers are not shown. One-sample two-sided Wilcoxon signed-rank test, with $\mu = 0$.

*(legend continued on next page)*

expression of mitotic genes to an extent comparable to the deletion of *Lin9,* confirming that they are regulated by YAP in KPL-CreER cells (Figure 1G). Additional direct targets of LIN9 such as *Aspm* and *Nusap1* were also downregulated after the depletion of YAP and TAZ. The decreased expression of the bona fide YAP-target genes *Cyr61* and *Sdpr* upon the depletion of YAP and TAZ confirmed that YAP and TAZ is active in these cells. Treatment of human A549 lung cancer cells with verteporfin, a drug that disrupts the YAP-TEAD interaction and leads to the inhibition of YAP-dependent gene expression (Brodowska et al., 2014), also resulted in the downregulation of mitotic MMB-target genes (Figure 1H). YAP protein levels, phosphorylation at S127, and nuclear localization, which are tightly regulated (Zhao et al., 2007), were unaffected by the deletion of *Lin9*, indicating that the effects of *Lin9* loss on the expression of YAP-target genes is not due to degradation or the nuclear exclusion of YAP (Figures S1B, S1D, and S1E).

## A Subset of YAP-Regulated Genes Are Direct Targets of MMB

We next performed chromatin immunoprecipitation sequencing (ChIP-seq) of LIN9 and YAP to better understand how MMB and YAP co-regulate mitotic genes in KPL-CreER cells. We found that there is relatively little overall overlap between LIN9 and YAP chromatin binding (Figures S2A–S2C). The majority of LIN9 peaks are located near transcriptional start sites (TSSs) of active promoters, whereas YAP mostly binds to intergenic enhancer and super-enhancer regions (Figures 2A and 2B). Comparison of the genomic localization of LIN9 with the TSSs of known YAP-target genes (Zanconato et al., 2015) showed that LIN9 binds to the promoter regions of a significant fraction of YAP-regulated genes (Figure 2C). Re-analysis of previously published datasets also confirmed that many YAP-target genes are bound by both DREAM and MMB-FOXM1 subunits (Fischer et al., 2016) (Figure S2D). The deletion of *Lin9* significantly downregulated the subset of YAP-target genes with LIN9 located at the promoter ($p = 0.000672$; Figure 2C; Table S1). In contrast, genes with a YAP peak in the promoter region, such as the well-described YAP targets *Ctgf*, *Cyr61*, and *Amotl2*, were not significantly downregulated by the deletion of *Lin9* (Figures 2C and S2E). Similar results were obtained by comparison with the conserved YAP signature described by Cordenonsi et al. (2011); specifically, 9 of 56 YAP signature genes are direct targets of LIN9 but have no YAP peak at the promoter (Figure 1C). Genome browser tracks of the targets *Cdc20*, *Cenpf*, and *Top2a* illustrating these findings are shown in Figures 2D and S2F.

## YAP Activates the Expression of Mitotic Genes in MCF10A Cells

The regulation of mitotic genes by YAP was further explored in untransformed human breast epithelial MCF10A cells expressing doxycycline-inducible YAP5SA, a constitutive active allele of YAP that cannot be inhibited by the Hippo kinases (von Eyss et al., 2015; Zhao et al., 2007) (Figure 3A). Genome-wide expression analysis by RNA sequencing revealed that a large number of genes are induced by YAP5SA in MCF10A cells, including known mitotic targets of MMB (Table S2). The upregulation of selected MMB-target genes by YAP5SA was confirmed independently by RT-qPCR (Figures 3B and S3A). ChIP-seq revealed that the majority of YAP peaks are located in enhancer regions, while LIN9 was highly enriched at open promoters (Figure 3C). The genomic localization of YAP and LIN9 in MCF10A cells was consistent with the localization of these factors in other cell types in published datasets (Figures S3B–S3E). YAP bound to the promoters of only a relatively small fraction (9%) of genes that are induced by YAP (94 of 1,027 genes). These direct YAP-target genes play roles in cell adhesion, cell junctions, and the actin cytoskeleton (Figure S4A). Conversely, LIN9 was highly enriched at the promoters of 245 YAP-induced genes (24%), and this set of YAP-induced/LIN9-bound genes was linked to ontological terms related to cell-cycle regulation and mitosis (Figure S4B).

Since the majority of YAP peaks are located in enhancer regions and because enhancer binding of YAP5SA stimulated enhancer activity as shown by the increased H3K27 acetylation levels at these sites (Figure S4C), we hypothesized that YAP activates MMB-target genes through long-range interactions from distant sites. With a published high-resolution chromatin interaction map (Hi-C) we were able to assign 5,018 YAP-bound enhancers identified by ChIP-seq to 2,771 promoters (Jin et al., 2013) (Figure 3D). LIN9 was highly enriched at 504 of these 2,711 promoters (Figure 3D). These LIN9-bound genes were significantly induced by YAP5SA ($p = 3.8 \times 10^{-6}$; Figure 3E). In stark contrast, genes that are associated with YAP-bound enhancers but do not have a LIN9 peak in the promoter were not significantly regulated by YAP5SA. Thus, binding of LIN9 to the TSS defines a set of cell-cycle genes that are activated by YAP from distant enhancers. Because LIN9 is a subunit of the MuvB core, which is part of the repressive DREAM complex and the activating MMB complex, the presence of LIN9 at the promoter does not explain how YAP5SA activates these genes. In fact, the induction of YAP5SA had little effect on the chromatin binding of LIN9 (Figure S4D). We therefore next assessed the binding of B-MYB, which is specific for the activating MuvB

(F) Empirical cumulative distribution function showing the recruitment of B-MYB upon YAP induction to LIN9-bound promoters linked to YAP-bound enhancers (n = 460). B-MYB reads were counted in a region of −100 to +400 bp relative to the TSS. The control group is defined as YAP-bound enhancers that loop to non-LIN9-bound promoters (n = 1,950).

(G) Scheme of long-range interactions of the *KIF23* promoter with distant loci as determined by 4C-seq, with the *KIF23* promoter as a viewpoint.

(H) Genome browser tracks around the *KIF23* locus (left) and downstream enhancers (right) illustrating the chromatin binding of the indicated proteins. YAP does not bind to the *KIF23* promoter, but it does bind to several up- and downstream enhancers labeled here as E1, E2, E3, and E4. Hi-C data showing long-range interactions between the *KIF23* promoter and YAP-bound enhancers are from Jin et al. (2013). Long-range interactions between the *KIF23* promoter and enhancers were determined by 4C-seq using the *KIF23* promoter as a viewpoint. The shading depicts the adjusted p values of significant contacts between the promoter and distant sites.

(I) Luciferase reporter assays of KIF23 enhancers E1–E4. Luciferase constructs were cotransfected with TEAD and YAP expression vectors. Activity was normalized to lysates of cells transfected with the empty pGL3 vector cotransfected with TEAD and YAP expression plasmids.

See also Figures S3, S4, and S5 and Table S2.

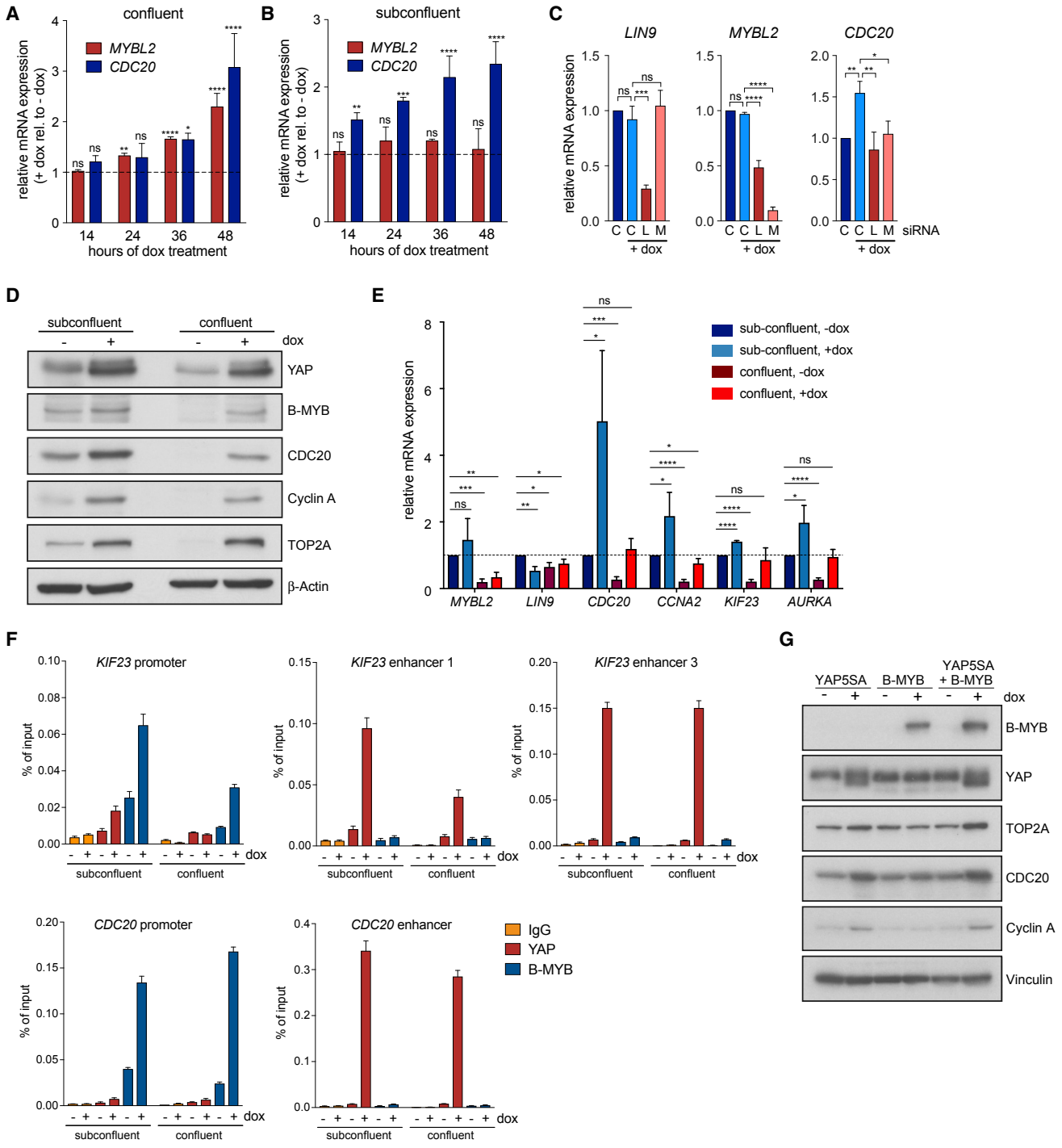


**Figure 4. YAP Induces the Expression and Chromatin Binding of B-MYB**

(A and B) Confluent (A) or subconfluent (B) MCF10A-YAP5SA cells were treated with 0.5 μg/mL doxycycline for the indicated times. Expression of *MYBL2* and *CDC20* relative to *GAPDH* was analyzed by RT-qPCR. Means and SDs of three biological replicates. Two-way ANOVA with Bonferroni's multiple comparison test.

(C) MCF10A-YAP5SA cells were transfected with a control siRNA (C) or with siRNAs specific for *LIN9* (L) or *MYBL2* (M). YAP5SA was induced by the addition of doxycycline. The expression of *LIN9*, *MYBL2*, and *CDC20* was analyzed by RT-qPCR. Means and SDs of three biological replicates. One-way ANOVA with Tukey's post-test.

(D) Subconfluent or confluent MCF10A-YAP5SA cells were treated with and without doxycycline for 48 h. The expression of the indicated proteins was analyzed by immunoblotting. β-Actin served as a control.

*(legend continued on next page)*

complex and which may provide an explanation for the activation of mitotic genes by YAP5SA (Figure 3F). Using ChIP-seq, we observed enhanced binding of B-MYB to LIN9-bound loci upon YAP5SA induction, suggesting a model in which YAP binding at enhancers promotes the chromatin association of B-MYB to promoter-bound LIN9, which in turn correlates with increased promoter activity, as determined by H3K27 acetylation (Figure S4D).

We next asked whether YAP interacts with the promoters of mitotic genes from distant enhancers through long-range interactions. To address this possibility, we performed circular chromosome conformation capture (4C-seq) assays with the promoters of three mitotic MMB-YAP-target genes (*AURKA*, *CDC20*, and *KIF23*) (Figures 3G, 3H, S5A, and S5B). By integrating 4C-seq and ChIP-seq data, four distal enhancers (E1–E4) that interact with the *KIF23* promoter were identified (Figures 3G and 3H). Upon doxycycline induction, YAP bound strongly to these four enhancers, and this was paralleled by the increased binding of B-MYB to the *KIF23* promoter (Figure 3H). Similarly, we identified a YAP-bound enhancer 50 kb upstream of the *AURKA* promoter and two enhancers located 150 kb upstream and 100 kb downstream of the *CDC20* promoter (Figures S5A and S5B). Binding of YAP to these enhancers also resulted in the increased binding of B-MYB to the corresponding promoters. We cloned the putative KIF23 enhancers E1–E4 in front of a minimal promoter driving the expression of luciferase. These enhancers, with the exception of E2, were activated upon YAP and TEAD coexpression, confirming the enhancer activity of the identified regions (Figure 3I).

## YAP Regulates the Expression of B-MYB and Promotes the Chromatin Binding of B-MYB

To determine whether YAP activates the expression of *MYBL2* and whether this contributes to the enhanced chromatin binding of B-MYB, we induced YAP5SA with doxycycline for different time periods and analyzed the expression of *MYBL2*. In confluent MCF10A cells, the mRNA and protein expression of B-MYB- and MMB-target genes was induced by YAP5SA (Figures 4A and 4D). In contrast, YAP5SA had no significant effect on the mRNA and protein expression of B-MYB in sparse, subconfluent MCF10A cultures, although the MMB target CDC20 was robustly induced in these conditions (Figures 4B and 4D). The induction of YAP5SA increased the fraction of cells in S and G2/M of the cell cycle in a TEAD-dependent manner, as evidenced by the inhibition of the YAP-TEAD interaction with verteporfin (Figure S5C). The YAP-induced increase in the expression of MMB-target genes was also inhibited by verteporfin (Figure S5D). Depletion of *LIN9* or *MYBL2* prevented the induction of *CDC20* by YAP5SA, indicating that this function of YAP is MMB dependent (Figure 4C). In MDA-MB-231 cells, which express high levels of YAP, the expression of B-MYB- and MMB-target genes was YAP dependent, further supporting a role for YAP in the expression and activity of B-MYB (Figure S5E).

In MCF10A cells, CDC20 mRNA and protein expression, as well as the expression of B-MYB and several other MMB targets, were downregulated when cells became confluent (Figures 4D and 4E). This likely reflects the lower levels of these genes in confluent cells due to repression by pocket protein-E2F complexes. More important, YAP5SA expression reverted the downregulation of mitotic genes in confluent MCF10A cells (Figures 4D and 4E). This re-activation of MMB targets by YAP5SA was paralleled by the increased binding of B-MYB to the promoters of genes co-regulated by YAP and MMB (Figures 4F and S5F). Although basal binding of B-MYB to target gene promoters was lower in confluent cells than in subconfluent cells (Figure S5G), the recruitment of B-MYB after YAP5SA induction was comparable in subconfluent and confluent cells (Figures 4F and S5F). This further supports the notion that YAP promotes the chromatin association of B-MYB independently from regulating B-MYB mRNA or protein expression and that this is a crucial step in the activation of target genes. Further support for such a model comes from the observations that the overexpression of B-MYB alone was not sufficient to induce the expression of MMB-target genes in the absence of exogenous YAP5SA and that B-MYB did not strongly synergize with YAP5SA in MCF10A cells (Figures 4G and S5H). Using ChIP, we found that YAP itself did not bind to the promoters of the analyzed genes, whereas it strongly bound to the 4C-identified enhancers (Figures 4F and S5F), validating the ChIP-seq data (see Figure 3). Taken together, YAP has the ability to activate MMB-target genes from distant enhancers, which is paralleled by increased binding of B-MYB to the promoters of genes co-regulated by YAP and MMB.

## YAP Activates the Expression of B-MYB from a Distal Enhancer

We next asked how YAP5SA activates the expression of *MYBL2*. Because our ChIP-seq assays indicated that YAP5SA does not directly bind to the *MYBL2* promoter, we asked whether YAP induces *MYBL2* expression through long-range chromatin interactions. Using 4C-seq, we detected a significant interaction between the *MYBL2* promoter and a distant enhancer (Figure S6A). YAP5SA robustly bound to this enhancer after the addition of doxycycline, which was validated by conventional ChIP (Figure S6B). The *MYBL2* enhancer contains a TEAD consensus element, further supporting the notion that it is regulated by YAP5SA. The binding of YAP5SA to the *MYBL2* enhancer stimulated enhancer activity, as indicated by increased acetylation

(E) MCF10A-YAP5SA cells were treated as in (D). The expression of the indicated genes relative to *GAPDH* was analyzed by RT-qPCR. Means and SDs of three biological replicates.

(F) Binding of YAP and B-MYB to the promoters and enhancers of *KIF23* and *CDC20* was analyzed by ChIP. Chromatin was isolated from subconfluent and confluent MCF10A cells before and after the induction of YAP5SA with 0.5 μg/mL doxycycline. Chromatin was immunoprecipitated with antisera specific for YAP or B-MYB. Nonspecific immunoglobulin G (IgG) served as a control. Additional promoters and enhancers are shown in Figure S5F.

(G) Subconfluent MCF10A-YAP5SA, MCF10A-B-MYB, or MCF10A-YAP5SA-B-MYB cells were treated with doxycycline to induce the expression of YAP5SA and/or B-MYB. Expression of the indicated proteins was analyzed by immunoblotting. Vinculin served as a control.

*$p < 0.05$; **$p < 0.01$; ***$p < 0.001$; ****$p < 0.0001$; ns, not significant, $p > 0.05$.

See also Figures S5 and S6.

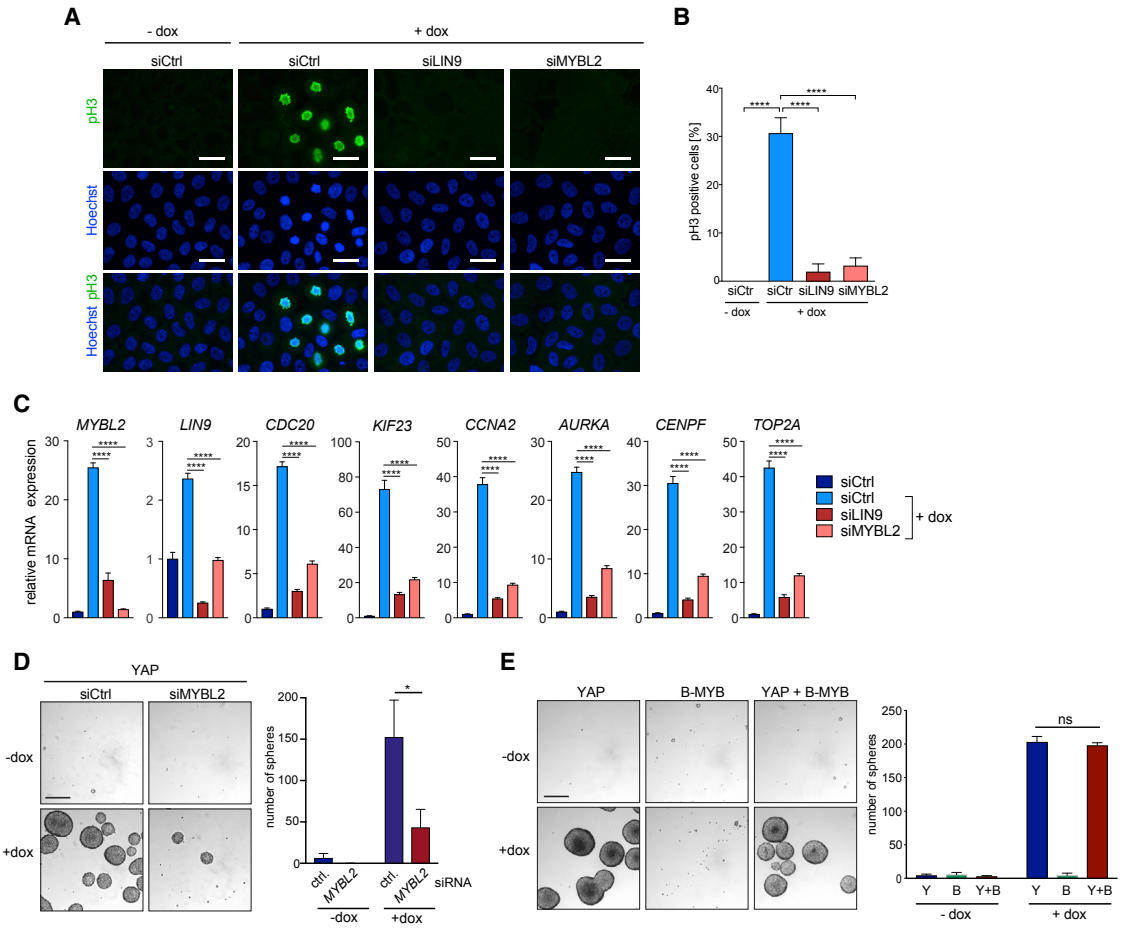


**Figure 5. MMB and YAP Functionally Interact**

(A) Serum-starved MCF10A-YAP5SA cells were transfected with a control siRNA or with siRNAs specific for *MYBL2* or *LIN9*. YAP was induced by the addition of doxycycline for 38 h, and cells in mitosis were analyzed by immunostaining for phosphorylated histone H3 (green). Nuclei are stained in blue. Bars: 25 μm.

(B) Quantification of $pH3^+$ cells in the experiment described in (A). Means and SDs of three biological replicates. Per experiment, at least 500 cells were analyzed. One-way ANOVA and Tukey's post-test.

(C) Serum-starved MCF10A-YAP5SA cells were treated as described in (A). The expression of the indicated genes relative to *GAPDH* was analyzed by RT-qPCR. n = 3 biological replicates. Shown are the means and SDs of three technical replicates of one representative example. One-way ANOVA followed by Tukey's post-test.

(D) Primary mammospheres formed by MCF10-YAP5SA cells transfected with a control siRNA or siRNA against *MYBL2*. YAP5SA expression was induced by the addition of doxycycline. Means and SDs of three biological replicates. Scale bar: 300 μm.

(E) Primary mammospheres formed by MCF10A-YAP5SA or MCF10A-B-MYB or MCF10A-YAP5SA + B-MYB cells. Expression of YAP5SA or B-MYB was induced by the addition of doxycycline. Data are means and SDs of three biological replicates. Scale bar: 300 μm.

See also Figure S6.

of H3K27 upon YAP binding (Figure S6A). These observations suggest that YAP stimulates the transcription of *MYBL2* from a distal enhancer through chromatin looping.

## MMB Is Required for YAP-Induced Cell-Cycle Progression

Next, we addressed the relevance of our findings for cell-cycle regulation. The activation of YAP5SA was sufficient to robustly stimulate the cell-cycle re-entry of serum-starved MCF10A cells as determined by staining for phosphorylated histone H3 (pH3), a marker of mitotic cells (Figures 5A and 5B). This pro-tumorigenic function of YAP5SA was reversed when *LIN9* or *MYBL2* was depleted by RNAi. The expression of *MYBL2* and of MMB-target genes increased strongly upon YAP5SA activation in starved cells in a B-MYB- and LIN9-dependent manner (Figure 5C). The ability of YAP5SA to increase the fraction of mitotic cells in unsynchronized, sparse cultures of MCF10A cells (i.e., in conditions in which no *MYBL2* expression is induced by YAP5SA) was also dependent on B-MYB (Figures S6C and S6D). To further investigate the contribution of MMB to oncogenic phenotypes mediated by YAP5SA, we next performed mammosphere assays. While the expression of YAP5SA resulted in the formation of numerous large spheres, the siRNA-mediated depletion of B-MYB significantly reduced mammosphere formation by

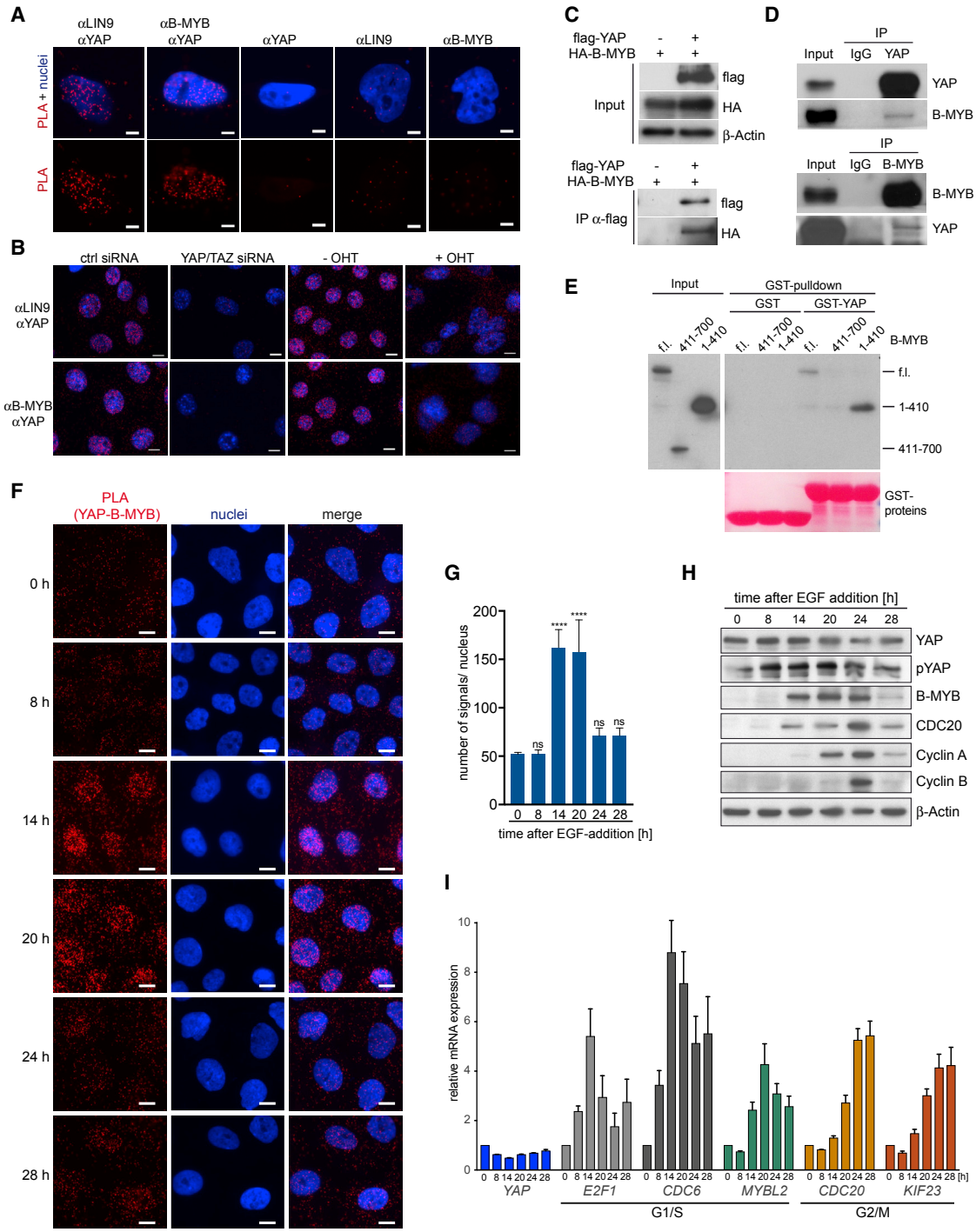


**Figure 6. YAP Physically Interacts with B-MYB**

(A) Proximity ligation assays (PLAs) of YAP and LIN9 and of YAP and B-MYB. Incubation with either YAP, LIN9, or B-MYB antibody alone was used as a control. Bars: 5 μm.

(B) PLA of YAP with LIN9 and with B-MYB in KPL-CreER cells. siRNA-mediated depletion of YAP and TAZ or Cre-mediated deletion of *Lin9* by 4-OHT served as control. Bars: 10 μm.

(C) Lysates of HeLa cells expressing HA-B-MYB and FLAG-tagged YAP were immunoprecipitated with FLAG antibodies and immunoblotted with FLAG and HA antibodies. IP, immunoprecipitation. Input: 2% of the amount used for IP was loaded on the gel.

(D) Nuclear lysates of KPL-CreER cells were immunoprecipitated with YAP antibodies (top) or B-MYB antibodies (bottom). Immunoprecipitation with nonspecific IgG served as a control. Input: 6.25% of IP amount was loaded.

*(legend continued on next page)*

YAP5SA (Figure 5D). The expression of B-MYB alone did not result in the formation of mammospheres, which is in agreement with the failure of B-MYB to induce the expression of MMB-target genes in the absence of YAP (Figures 4G and 5E). Collectively, our data indicate that MMB is required for the activation of essential cell-cycle genes by YAP.

### YAP Physically Interacts with MMB

Given that our data suggest that YAP interacts with MMB from distant enhancers, we next asked whether MMB and YAP physically interact. Using the *in situ* proximity ligation assay (PLA), we found that interactions between YAP and the MMB subunits LIN9 and B-MYB were readily detected in the nucleus (Figure 6A). These interactions were specific, because no signal was observed when one of the two antibodies was omitted. The PLA signal was lost when *Yap* and *Taz* were depleted by siRNA or when *Lin9* was deleted (Figure 6B). That MMB and YAP interact was confirmed by co-immunoprecipitation of hemagglutinin-B-MYB (HA-B-MYB) with FLAG-YAP from the lysates of cells transfected with these constructs (Figure 6C). The endogenous proteins also interacted, as B-MYB was co-immunoprecipitated with endogenous YAP and vice versa (Figure 6D). In glutathione S-transferase (GST)-pull-down experiments, we found that full-length B-MYB and the N terminus of B-MYB (1–410), but not the C terminus of B-MYB (411–700), interact with YAP, indicating that binding of B-MYB to YAP is independent from the C-terminal MuvB-binding domain of B-MYB (Guiley et al., 2018) (Figure 6E). During cell-cycle progression of MCF10A cells (Figure S6E), endogenous YAP and B-MYB associate in late G1 and S phases (Figures 6F and 6G) just before the activation of YAP-MMB-target genes, which is consistent with the coactivation of these genes by YAP and B-MYB and is independent from changes in Ser127 phosphorylation of YAP (Figure 6H). Entry of MCF10A cells into G2/M and the induction of B-MYB- and MMB-target genes was YAP and MMB dependent (Figures S6F–S6I), supporting a role for YAP and MMB in activating a common set of target genes important for cell-cycle progression.

### Clinical Relevance of MMB-Dependent YAP-Target Genes

Finally, we asked whether the common MMB- and YAP-target genes are of any clinical significance for cancer. We first analyzed whether YAP-target genes are co-expressed with *MYBL2* mRNA by examining previously published microarray datasets. In non-small-cell lung cancer, the expression of YAP-target genes significantly correlated with *MYBL2* expression (Figures 7A and 7B). Consistent with these findings, YAP and B-MYB protein expression was positively correlated in human lung adenocarcinomas, as determined by immunohistochemistry (Figure 7C). YAP and B-MYB were also co-expressed in murine lung adenocarcinomas (Figure S7A). Moreover, in human lung tumors, the expression of genes that are LIN9 bound and loop to a YAP-bound enhancer ("YAP-MMB targets") correlated with the expression of *MYBL2* (Figure 7D). Notably, *MYBL2* and YAP-MMB-target genes were expressed at higher levels in tumors as compared to normal tissue. Patients with elevated expression levels of YAP-MMB-target genes showed a significant shorter survival compared to patients with lower expression of these genes. In contrast, the expression of genes with a YAP peak in the promoter ("YAP direct targets") did not correlate with *MYBL2* expression and was not increased in tumors compared to normal tissue (Figure 7E). The expression of direct YAP targets also did not stratify the survival of lung adenocarcinoma patients. GSEA showed that these findings are not limited to lung cancer: YAP-MMB-target genes are enriched in several tumor entities and discriminate tumor tissue from normal tissue or late tumor stages from early stages (Figure S7B). In contrast, YAP-direct targets are not significantly enriched in more advanced tumors. In fact, in several entities, YAP-direct target genes are depleted in cancer tissues or late-stage cancer compared to normal tissues or early-stage cancers, respectively. We conclude that the activation of YAP-MMB-target genes establishes an oncogenic gene expression signature in several tumor entities and may allow the discrimination of advanced from less aggressive tumors.

## DISCUSSION

A key feature of the Hippo-YAP pathway is its interconnection with other cellular pathways (Irvine, 2012). Here, we report a link between the coactivator YAP and the MMB complex, an activator of cell-cycle genes expressed in G2/M, broadening the current knowledge about the regulation of mitotic progression by YAP. It is well established that YAP is a powerful inducer of cellular proliferation. Previous studies have shown that E2F and MYC transcription factors are critical regulators of YAP-induced cell-cycle gene activation. For example, YAP and E2F co-regulate cell-cycle genes in the liver (Ehmer et al., 2014). Furthermore, YAP has been shown to cooperate with MYC in the cell-cycle entry of serum-starved, confluent cells (Croci et al., 2017). We report that MMB is required for YAP to activate a set of genes that are involved in the completion of mitosis. By performing genome-wide expression and binding analyses, we found that YAP modulates MMB activity by at least two different mechanisms: transcriptional control of B-MYB expression and regulation of B-MYB chromatin binding. In serum-starved or highly confluent cells, YAP activated the expression of B-MYB to induce mitotic genes. It remains to be shown whether the activation of B-MYB by YAP involves E2F transcription factors,

(E) Immobilized recombinant GST or GST-WW1/2-YAP was incubated with the indicated HA-tagged B-MYB constructs. Bound HA-B-MYB was detected by immunoblotting.
(F) PLA of YAP and B-MYB in serum-starved MCF10A cells that were treated with 20 ng/mL epidermal growth factor (EGF) for the indicated times. n = 2 independent replicates. Bars: 10 μm.
(G) Quantification of PLA shown in (F). Error bars show SDs of technical triplicates from one representative experiment (n = 2).
(H and I) The expression of YAP, B-MYB, G1/S, and G2/M genes after EGF-mediated cell-cycle re-entry of starved MCF10A cells was analyzed by immunoblotting (H) and RT-qPCR (I). Error bars show SD of technical triplicates from one representative experiment (n = 2).
See also Figure S6.

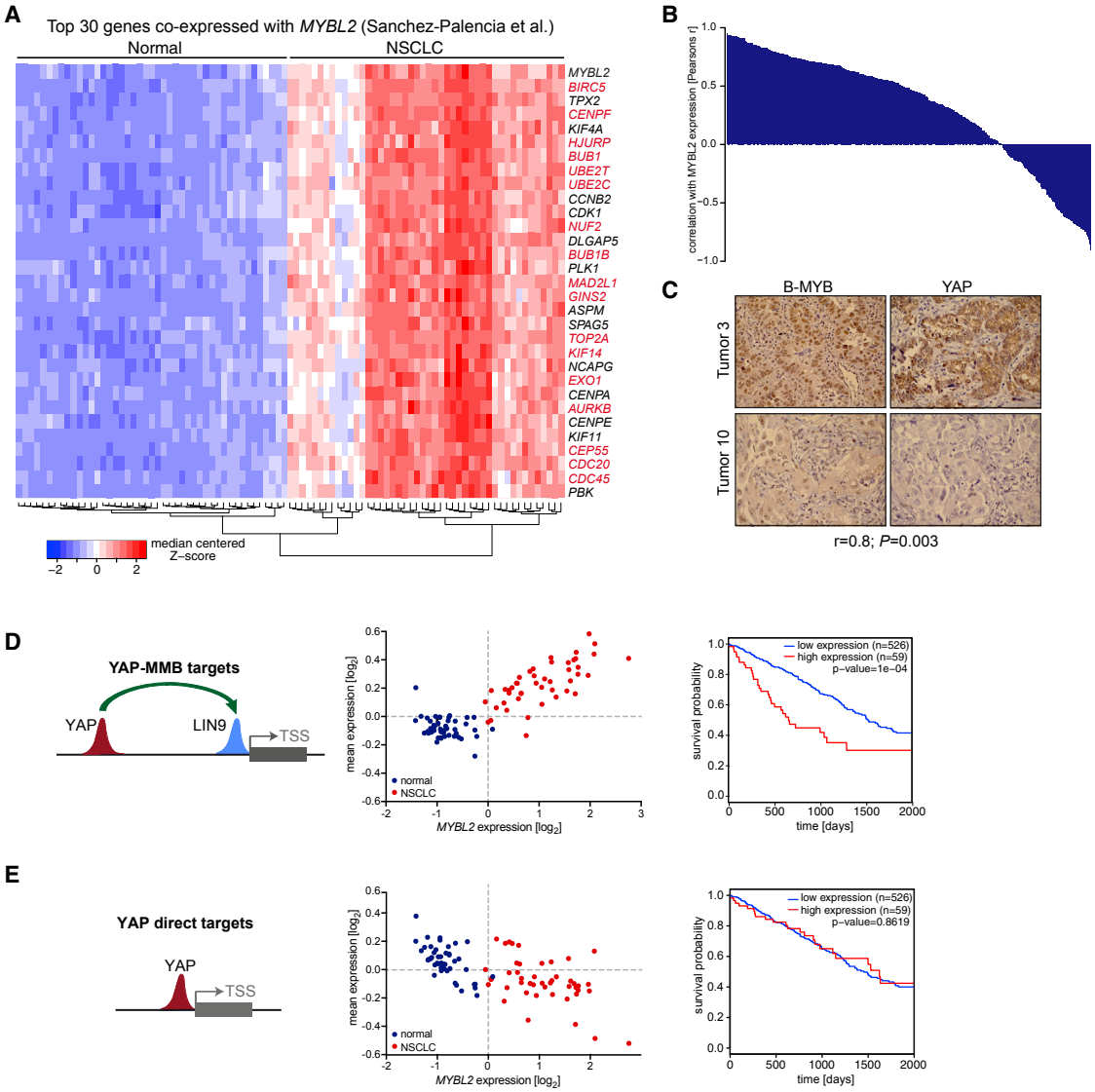


**Figure 7. Genes Co-regulated by MMB and YAP Are Relevant for Cancer**

(A) Analysis of genes co-expressed with *MYBL2* in non-small-cell lung cancer (NSCLC) (GSE18842; Sanchez-Palencia et al., 2011). The top 30 genes co-expressed with *MYBL2* are shown. Known YAP-target genes are depicted in red.

(B) Waterfall plot depicting the correlation coefficients of *MYBL2* with YAP-target genes from Zanconato et al. (2015) in the lung cancer dataset GSE18842 (Sanchez-Palencia et al., 2011).

(C) The expression of B-MYB (phospho-T487) and YAP in 11 human lung adenocarcinomas was determined by immunohistochemistry and scored from 0 to 3. The expression of B-MYB (phospho-T487) and YAP was significantly correlated (Pearson's r = 0.80, p = 0.003). Representative stainings of tumors with high (tumor 3) and low (tumor 10) expression of B-MYB and YAP are shown.

(D and E) Correlation of *MYBL2* expression and survival in lung cancer patients with expression of YAP-MMB targets (genes that are LIN9 bound and loop to a YAP-bound enhancer; n = 443) (D) or with YAP-direct targets (genes that have a YAP peak ±0.5 kb from their TSS; n = 404) (E). Normal tissue is shown in blue. NSCLC is shown in red. Kaplan-Meier plots show overall survival of lung adenocarcinoma patients (TCGA) in the dataset GSE18842.

See also Figure S7.

which have been implicated in activating the MYBL2 promoter (Liu et al., 1996). B-MYB is not only a downstream target gene of YAP but also physically interacts with YAP. This interaction promotes the association of B-MYB with genomic loci prebound by MuvB, leading to the transcriptional activation of mitotic YAP target genes. Mechanistically, YAP does not cooperate with MMB by co-binding to the same promoters, but instead acts from distant enhancer elements, which is consistent with recent reports that YAP mainly activates genes from distal sites (Cebola et al., 2015; Galli et al., 2015; Zanconato et al., 2015). Thus, YAP interacts with B-MYB-target promoters by chromatin looping, a model that is supported by 4C-seq assays (Figures 3G and 3H).

YAP induction does not affect looping (data not shown), but instead functions to increase B-MYB occupancy at MuvB promoter elements.

Previous studies have described a connection between the Hippo pathway and MuvB in cell-cycle control. Specifically, it has been shown that the Hippo kinase LATS2 stimulates the kinase activity of DYRK1A to phosphorylate the MuvB subunit LIN52 and promote the assembly of the repressive DREAM complex (Litovchick et al., 2011; Tschöp et al., 2011). This mechanism plays an important role in the inhibition of cell proliferation and entry into quiescence. Our results reported here extend these observations by showing that Hippo signaling, through its downstream effector YAP and independently from DYRK1A, also affects MuvB by regulating B-MYB. These findings suggest that the loss of Hippo signaling in cancer cells affects the two major sets of cell-cycle genes with peak expression in either G1/S or in G2/M by its ability to regulate MuvB. First, in Hippo-deficient cells, the absence of LATS2-mediated activation of DYRK1A interferes with DREAM assembly, resulting in the derepression of E2F-regulated G1/S genes. Second, high levels of YAP in Hippo-deficient cells promote B-MYB activity, leading to the activation of genes expressed in G2/M. Both mechanisms are expected to contribute to the loss of proliferation control in Hippo-deficient cancer cells. Unrestrained activity of genes co-regulated by YAP and MMB involved in mitotic progression may not only promote proliferation but also lead to chromosomal instability (CIN) and aneuploidy, which are tightly associated with tumorigenesis (Bakhoum and Compton, 2012). In this regard, several mitotic genes induced by YAP and B-MYB, including *CDC20*, *TOP2A*, and *ECT2*, are part of a signature of 70 genes whose elevated expression is associated with CIN and a poor prognosis across several different cancer types (Carter et al., 2006). Furthermore, the expression of genes coactivated by YAP and B-MYB is associated with the poor survival of lung cancer patients (Figure 7D). Disrupting the interaction between the MMB and Hippo-YAP pathway may therefore be a novel therapeutic strategy for the treatment of cancer.

## STAR★METHODS

Detailed methods are provided in the online version of this paper and include the following:

- KEY RESOURCES TABLE
- CONTACT FOR REAGENT AND RESOURCE SHARING
- EXPERIMENTAL MODEL AND SUBJECT DETAILS
  - Cell lines
- METHOD DETAILS
  - Lentiviral production and infection
  - siRNA transfection
  - Mammosphere assays
  - RT-qPCR
  - ChIP and ChIP-sequencing
  - RNA-seq analysis
  - Immunoblotting and immunoprecipitation
  - GST-pulldown assays
  - Subcellular fractionation
  - Luciferase assays
  - PLA
  - Circular Chromosome Conformation Capture assays (4C-seq)
  - Immunostaining and immunohistochemistry
  - Gene set enrichment analysis (GSEA)
  - Bioinformatics
- QUANTIFICATION AND STATISTICAL ANALYSIS
- DATA AND SOFTWARE AVAILABILITY

### SUPPLEMENTAL INFORMATION

Supplemental Information can be found online at https://doi.org/10.1016/j.celrep.2019.05.071.

### ACKNOWLEDGMENTS

We thank Roger Watson and James DeCaprio for sharing antibodies. We thank Susi Spahr and Ashley Curran for assistance. This work was supported by grants from the Deutsche Krebshilfe (110928) and Sander Stiftung (2015.038.2) (to S.G.). We acknowledge financial support by the Deutsche Forschungsgemeinschaft within the funding program Open Access Publishing and by the University of Wuerzburg. B.v.E. was supported by grants from the Else Kröner Foundation (2016_A58) and the Deutsche Krebshilfe (70113138). The Fritz Lipmann Institute (FLI) is a member of the Leibniz Association and is financially supported by the Federal Government of Germany and the State of Thuringia.

### AUTHOR CONTRIBUTIONS

S.G. and G.P. planned the study. G.P., B.v.E., and S.G. designed the experiments. G.P., M.S., E.R., M.G., A.C.-V., and S.G. conducted the experiments. G.P., M.S., and S.G. analyzed the data. S.K. performed the initial analysis of the murine ChIP-seq data. S.W. and B.v.E. performed the bioinformatic analyses. A.R. analyzed the human pathological samples. A.B., C.P.A., and E.W. performed and supervised the next-generation sequencing. S.G. and G.P. wrote the manuscript.

### DECLARATION OF INTERESTS

The authors declare no competing interests.

Received: December 18, 2018
Revised: April 18, 2019
Accepted: May 17, 2019
Published: June 18, 2019

### SUPPORTING CITATIONS

The following reference appears in the Supplemental Information: Jang et al. (2017).

### REFERENCES

Bai, H., Gayyed, M.F., Lam-Himlin, D.M., Klein, A.P., Nayar, S.K., Xu, Y., Khan, M., Argani, P., Pan, D., and Anders, R.A. (2012). Expression of Yes-associated protein modulates Survivin expression in primary liver malignancies. Hum. Pathol. *43*, 1376–1385.

Bakhoum, S.F., and Compton, D.A. (2012). Chromosomal instability and cancer: a complex relationship with therapeutic potential. J. Clin. Invest. *122*, 1138–1143.

Brodowska, K., Al-Moujahed, A., Marmalidou, A., Meyer Zu Horste, M., Cichy, J., Miller, J.W., Gragoudas, E., and Vavvas, D.G. (2014). The clinically used photosensitizer Verteporfin (VP) inhibits YAP-TEAD and human retinoblastoma cell growth in vitro without light activation. Exp. Eye Res. *124*, 67–73.

Carter, S.L., Eklund, A.C., Kohane, I.S., Harris, L.N., and Szallasi, Z. (2006). A signature of chromosomal instability inferred from gene expression profiles predicts clinical outcome in multiple human cancers. Nat. Genet. *38*, 1043–1048.

Cebola, I., Rodríguez-Seguí, S.A., Cho, C.H.-H., Bessa, J., Rovira, M., Luengo, M., Chhatriwala, M., Berry, A., Ponsa-Cobas, J., Maestro, M.A., et al. (2015). TEAD and YAP regulate the enhancer network of human embryonic pancreatic progenitors. Nat. Cell Biol. *17*, 615–626.

Cordenonsi, M., Zanconato, F., Azzolin, L., Forcato, M., Rosato, A., Frasson, C., Inui, M., Montagner, M., Parenti, A.R., Poletti, A., et al. (2011). The Hippo transducer TAZ confers cancer stem cell-related traits on breast cancer cells. Cell *147*, 759–772.

Croci, O., De Fazio, S., Biagioni, F., Donato, E., Caganova, M., Curti, L., Doni, M., Sberna, S., Aldeghi, D., Biancotto, C., et al. (2017). Transcriptional integration of mitogenic and mechanical signals by Myc and YAP. Genes Dev. *31*, 2017–2022.

Dupont, S., Morsut, L., Aragona, M., Enzo, E., Giulitti, S., Cordenonsi, M., Zanconato, F., Le Digabel, J., Forcato, M., Bicciato, S., et al. (2011). Role of YAP/TAZ in mechanotransduction. Nature *474*, 179–183.

Edgar, R., Domrachev, M., and Lash, A.E. (2002). Gene Expression Omnibus: NCBI gene expression and hybridization array data repository. Nucleic Acids Res. *30*, 207–210.

Ehmer, U., Zmoos, A.-F., Auerbach, R.K., Vaka, D., Butte, A.J., Kay, M.A., and Sage, J. (2014). Organ size control is dominant over Rb family inactivation to restrict proliferation in vivo. Cell Rep. *8*, 371–381.

von Eyss, B., Jaenicke, L.A., Kortlever, R.M., Royla, N., Wiese, K.E., Letschert, S., McDuffus, L.-A., Sauer, M., Rosenwald, A., Evan, G.I., et al. (2015). A MYC-Driven Change in Mitochondrial Dynamics Limits YAP/TAZ Function in Mammary Epithelial Cells and Breast Cancer. Cancer Cell *28*, 743–757.

Fischer, M., and Müller, G.A. (2017). Cell cycle transcription control: DREAM/MuvB and RB-E2F complexes. Crit. Rev. Biochem. Mol. Biol. *52*, 638–662.

Fischer, M., Grossmann, P., Padi, M., and DeCaprio, J.A. (2016). Integration of TP53, DREAM, MMB-FOXM1 and RB-E2F target gene analyses identifies cell cycle gene regulatory networks. Nucleic Acids Res. *44*, 6070–6086.

Galli, G.G., Carrara, M., Yuan, W.-C., Valdes-Quezada, C., Gurung, B., Pepe-Mooney, B., Zhang, T., Geeven, G., Gray, N.S., de Laat, W., et al. (2015). YAP Drives Growth by Controlling Transcriptional Pause Release from Dynamic Enhancers. Mol. Cell *60*, 328–337.

Guiley, K.Z., Iness, A.N., Saini, S., Tripathi, S., Lipsick, J.S., Litovchick, L., and Rubin, S.M. (2018). Structural mechanism of Myb-MuvB assembly. Proc. Natl. Acad. Sci. USA *115*, 10016–10021.

Hong, W., and Guan, K.-L. (2012). The YAP and TAZ transcription co-activators: key downstream effectors of the mammalian Hippo pathway. Semin. Cell Dev. Biol. *23*, 785–793.

Huang, W., Sherman, B.T., and Lempicki, R.A. (2009). Systematic and integrative analysis of large gene lists using DAVID bioinformatics resources. Nat. Protoc. *4*, 44–57.

Iltzsche, F., Simon, K., Stopp, S., Pattschull, G., Francke, S., Wolter, P., Hauser, S., Murphy, D.J., García, P., Rosenwald, A., and Gaubatz, S. (2017). An important role for Myb-MuvB and its target gene KIF23 in a mouse model of lung adenocarcinoma. Oncogene *36*, 110–121.

Irvine, K.D. (2012). Integration of intercellular signaling through the Hippo pathway. Semin. Cell Dev. Biol. *23*, 812–817.

Jang, W., Kim, T., Koo, J.S., Kim, S.-K., and Lim, D.-S. (2017). Mechanical cue-induced YAP instructs Skp2-dependent cell cycle exit and oncogenic signaling. EMBO J. *36*, 2510–2528.

Jin, F., Li, Y., Dixon, J.R., Selvaraj, S., Ye, Z., Lee, A.Y., Yen, C.-A., Schmitt, A.D., Espinoza, C.A., and Ren, B. (2013). A high-resolution map of the three-dimensional chromatin interactome in human cells. Nature *503*, 290–294.

Kapoor, A., Yao, W., Ying, H., Hua, S., Liewen, A., Wang, Q., Zhong, Y., Wu, C.-J., Sadanandam, A., Hu, B., et al. (2014). Yap1 activation enables bypass of oncogenic Kras addiction in pancreatic cancer. Cell *158*, 185–197.

Kim, D., Pertea, G., Trapnell, C., Pimentel, H., Kelley, R., and Salzberg, S.L. (2013). TopHat2: accurate alignment of transcriptomes in the presence of insertions, deletions and gene fusions. Genome Biol. *14*, R36.

Lange, A.W., Sridharan, A., Xu, Y., Stripp, B.R., Perl, A.-K., and Whitsett, J.A. (2015). Hippo/Yap signaling controls epithelial progenitor cell proliferation and differentiation in the embryonic and adult lung. J. Mol. Cell Biol. *7*, 35–47.

Langmead, B., and Salzberg, S.L. (2012). Fast gapped-read alignment with Bowtie 2. Nat. Methods *9*, 357–359.

Langmead, B., Trapnell, C., Pop, M., and Salzberg, S.L. (2009). Ultrafast and memory-efficient alignment of short DNA sequences to the human genome. Genome Biol. *10*, R25.

Litovchick, L., Sadasivam, S., Florens, L., Zhu, X., Swanson, S.K., Velmurugan, S., Chen, R., Washburn, M.P., Liu, X.S., and DeCaprio, J.A. (2007). Evolutionarily conserved multisubunit RBL2/p130 and E2F4 protein complex represses human cell cycle-dependent genes in quiescence. Mol. Cell *26*, 539–551.

Litovchick, L., Florens, L.A., Swanson, S.K., Washburn, M.P., and DeCaprio, J.A. (2011). DYRK1A protein kinase promotes quiescence and senescence through DREAM complex assembly. Genes Dev. *25*, 801–813.

Liu, N., Lucibello, F.C., Zwicker, J., Engeland, K., and Müller, R. (1996). Cell cycle-regulated repression of B-myb transcription: cooperation of an E2F site with a contiguous corepressor element. Nucleic Acids Res. *24*, 2905–2910.

Meng, Z., Moroishi, T., and Guan, K.-L. (2016). Mechanisms of Hippo pathway regulation. Genes Dev. *30*, 1–17.

Osterloh, L., von Eyss, B., Schmit, F., Rein, L., Hübner, D., Samans, B., Hauser, S., and Gaubatz, S. (2007). The human synMuv-like protein LIN-9 is required for transcription of G2/M genes and for entry into mitosis. EMBO J. *26*, 144–157.

Pilkinton, M., Sandoval, R., and Colamonici, O.R. (2007). Mammalian Mip/LIN-9 interacts with either the p107, p130/E2F4 repressor complex or B-Myb in a cell cycle-phase-dependent context distinct from the Drosophila dREAM complex. Oncogene *26*, 7535–7543.

Quinlan, A.R., and Hall, I.M. (2010). BEDTools: a flexible suite of utilities for comparing genomic features. Bioinformatics *26*, 841–842.

Ramírez, F., Dündar, F., Diehl, S., Grüning, B.A., and Manke, T. (2014). deepTools: a flexible platform for exploring deep-sequencing data. Nucleic Acids Res. *42*, W187-91.

Reichert, N., Wurster, S., Ulrich, T., Schmitt, K., Hauser, S., Probst, L., Götz, R., Ceteci, F., Moll, R., Rapp, U., and Gaubatz, S. (2010). Lin9, a subunit of the mammalian DREAM complex, is essential for embryonic development, for survival of adult mice, and for tumor suppression. Mol. Cell. Biol. *30*, 2896–2908.

Robinson, M.D., McCarthy, D.J., and Smyth, G.K. (2010). edgeR: a Bioconductor package for differential expression analysis of digital gene expression data. Bioinformatics *26*, 139–140.

Robinson, J.T., Thorvaldsdóttir, H., Winckler, W., Guttman, M., Lander, E.S., Getz, G., and Mesirov, J.P. (2011). Integrative genomics viewer. Nat. Biotechnol. *29*, 24–26.

Sadasivam, S., and DeCaprio, J.A. (2013). The DREAM complex: master coordinator of cell cycle-dependent gene expression. Nat. Rev. Cancer *13*, 585–595.

Sadasivam, S., Duan, S., and DeCaprio, J.A. (2012). The MuvB complex sequentially recruits B-Myb and FoxM1 to promote mitotic gene expression. Genes Dev. *26*, 474–489.

Sanchez-Palencia, A., Gomez-Morales, M., Gomez-Capilla, J.A., Pedraza, V., Boyero, L., Rosell, R., and Fárez-Vidal, M.E. (2011). Gene expression profiling reveals novel biomarkers in nonsmall cell lung cancer. Int. J. Cancer *129*, 355–364.

Schmit, F., Korenjak, M., Mannefeld, M., Schmitt, K., Franke, C., von Eyss, B., Gagrica, S., Hänel, F., Brehm, A., and Gaubatz, S. (2007). LINC, a human complex that is related to pRB-containing complexes in invertebrates regulates the expression of G2/M genes. Cell Cycle *6*, 1903–1913.

Stadhouders, R., Kolovos, P., Brouwer, R., Zuin, J., van den Heuvel, A., Kockx, C., Palstra, R.-J., Wendt, K.S., Grosveld, F., van Ijcken, W., and Soler, E.

(2013). Multiplexed chromosome conformation capture sequencing for rapid genome-scale high-resolution detection of long-range chromatin interactions. Nat. Protoc. *8*, 509–524.

Stein, C., Bardet, A.F., Roma, G., Bergling, S., Clay, I., Ruchti, A., Agarinis, C., Schmelzle, T., Bouwmeester, T., Schübeler, D., and Bauer, A. (2015). YAP1 Exerts Its Transcriptional Control via TEAD-Mediated Activation of Enhancers. PLoS Genet. *11*, e1005465.

Subramanian, A., Tamayo, P., Mootha, V.K., Mukherjee, S., Ebert, B.L., Gillette, M.A., Paulovich, A., Pomeroy, S.L., Golub, T.R., Lander, E.S., and Mesirov, J.P. (2005). Gene set enrichment analysis: a knowledge-based approach for interpreting genome-wide expression profiles. Proc. Natl. Acad. Sci. USA *102*, 15545–15550.

Tavner, F., Frampton, J., and Watson, R.J. (2007). Targeting an E2F site in the mouse genome prevents promoter silencing in quiescent and post-mitotic cells. Oncogene *26*, 2727–2735.

Tremblay, A.M., Missiaglia, E., Galli, G.G., Hettmer, S., Urcia, R., Carrara, M., Judson, R.N., Thway, K., Nadal, G., Selfe, J.L., et al. (2014). The Hippo transducer YAP1 transforms activated satellite cells and is a potent effector of embryonal rhabdomyosarcoma formation. Cancer Cell *26*, 273–287.

Tschöp, K., Conery, A.R., Litovchick, L., Decaprio, J.A., Settleman, J., Harlow, E., and Dyson, N. (2011). A kinase shRNA screen links LATS2 and the pRB tumor suppressor. Genes Dev. *25*, 814–830.

Whyte, W.A., Orlando, D.A., Hnisz, D., Abraham, B.J., Lin, C.Y., Kagey, M.H., Rahl, P.B., Lee, T.I., and Young, R.A. (2013). Master transcription factors and mediator establish super-enhancers at key cell identity genes. Cell *153*, 307–319.

Xu, S., Grullon, S., Ge, K., and Peng, W. (2014). Spatial clustering for identification of ChIP-enriched regions (SICER) to map regions of histone methylation patterns in embryonic stem cells. Methods Mol. Biol. *1150*, 97–111.

Zanconato, F., Forcato, M., Battilana, G., Azzolin, L., Quaranta, E., Bodega, B., Rosato, A., Bicciato, S., Cordenonsi, M., and Piccolo, S. (2015). Genome-wide association between YAP/TAZ/TEAD and AP-1 at enhancers drives oncogenic growth. Nat. Cell Biol. *17*, 1218–1227.

Zhang, Y., Liu, T., Meyer, C.A., Eeckhoute, J., Johnson, D.S., Bernstein, B.E., Nusbaum, C., Myers, R.M., Brown, M., Li, W., and Liu, X.S. (2008). Model-based analysis of ChIP-Seq (MACS). Genome Biol. *9*, R137.

Zhang, H., Liu, C.-Y., Zha, Z.-Y., Zhao, B., Yao, J., Zhao, S., Xiong, Y., Lei, Q.-Y., and Guan, K.-L. (2009). TEAD transcription factors mediate the function of TAZ in cell growth and epithelial-mesenchymal transition. J. Biol. Chem. *284*, 13355–13362.

Zhao, B., Wei, X., Li, W., Udan, R.S., Yang, Q., Kim, J., Xie, J., Ikenoue, T., Yu, J., Li, L., et al. (2007). Inactivation of YAP oncoprotein by the Hippo pathway is involved in cell contact inhibition and tissue growth control. Genes Dev. *21*, 2747–2761.

Zhao, B., Ye, X., Yu, J., Li, L., Li, W., Li, S., Yu, J., Lin, J.D., Wang, C.-Y., Chinnaiyan, A.M., et al. (2008). TEAD mediates YAP-dependent gene induction and growth control. Genes Dev. *22*, 1962–1971.

## STAR★METHODS

### KEY RESOURCES TABLE

| REAGENT or RESOURCE | SOURCE | IDENTIFIER |
|---|---|---|
| Antibodies | | |
| Mouse monoclonal anti-β-Actin | Santa Cruz Biotechnology | Cat# sc-47778; RRID: AB_626632 |
| Rabbit polyclonal anti-B-MYB | Santa Cruz Biotechnology | Cat# sc-724; RRID: AB_631985 |
| Mouse monoclonal anti-B-MYB (clone LX015.1) | Gift from Roger Watson | N/A |
| Rabbit monoclonal anti B-MYB (phospho T487) | Abcam | Cat# ab-76009; RRID: AB_1309969 |
| Mouse monoclonal anti-CDC20 | Santa Cruz Biotechnology | Cat# sc-13162; RRID: AB_628089 |
| Mouse monoclonal anti-Cyclin A | Santa Cruz Biotechnology | Cat# sc-239; RRID: AB_627334 |
| Mouse monoclonal anti-Cyclin B1 | Santa Cruz Biotechnology | Cat# sc-245; RRID: AB_627338 |
| Mouse monoclonal anti-FLAG M2 | Sigma | Cat# F3165; RRID: AB_259529 |
| Mouse monoclonal anti-HA.11 | Covance | Cat# MMS-101P; RRID: AB_2314672 |
| Rabbit polyclonal anti-Histone H2B | Abcam | Cat# ab1790; RRID: AB302612 |
| Rabbit polyclonal anti-Histone H3 (mono methyl K4) | Abcam | Cat# ab8895; RRID: AB_306847 |
| Rabbit polyclonal anti-Histone H3 (tri methyl K4) | Abcam | Cat# ab8580; RRID: AB_306649 |
| Rabbit polyclonal anti Histone H3 (K27 acetyl) | Merck | Cat# 07-360; RRID: AB_310550 |
| Rabbit polyclonal anti-phospho-Histone H3 (Ser10) | Santa Cruz Biotechnology | Cat# sc-8656-R; RRID: AB_653256 |
| IgG from rabbit serum | Sigma | Cat# I5006; RRID: AB_1163659 |
| Rabbit polyclonal anti-LIN9 | Bethyl | Cat# A300-BL2981; RRID: N/A |
| Mouse monoclonal anti-TOP2A | Santa Cruz Biotechnology | Cat# sc-365916; RRID: AB_10842059 |
| Mouse monoclonal anti-α-Tubulin | Santa Cruz Biotechnology | Cat# sc-23948; RRID: AB_628410 |
| Mouse monoclonal anti-Vinculin | Sigma | Cat# V9131; RRID: AB_477629 |
| Rabbit polyclonal anti-YAP | Novus | Cat# NB110-58358; RRID: AB_922796 |
| Mouse monoclonal anti-YAP | Santa Cruz Biotechnology | Cat# sc-101199;RRID: AB_1131430 |
| Rabbit monoclonal anti-YAP | Cell Signaling Technology | Cat# 14074; RRID: AB_2650491 |
| Rabbit polyclonal anti-YAP | Cell Signaling Technology | Cat# 4912; RRID: AB_2218911 |
| Rabbit polylonal anti-phospho-YAP (Ser127) | Cell Signaling Technology | Cat# 4911; RRID: AB_2218913 |
| Anti-mouse IgG (H+L) Alexa Fluor 488 | Thermo Fisher Scientific | Cat# A-11029; RRID: AB_138404 |
| Anti-rabbit IgG (H+L) Alexa Fluor 488 | Thermo Fisher Scientific | Cat# A-21206; RRID: AB_141708 |
| Anti-rabbit IgG (H+L) Alexa Fluor 594 | Thermo Fisher Scientific | Cat# A-11037; RRID: AB_2534095 |
| Anti-mouse HRP conjugated | GE Healthcare | Cat# NXA931; RRID: AB_772209 |
| Anti-rabbit HRP conjugated | Thermo Fisher | Cat# 656120;RRID: AB_2533967 |
| HRP Protein A | BD Biosciences | Cat# 610438; RRID: N/A |
| Mouse TrueBlot ULTRA: Anti-Mouse Ig HRP | Rockland | Cat# 18-8817-30; RRID: AB_2610849 |
| Bacterial and Virus Strains | | |
| *Escherichia coli* BL21 (DE3) pLysS | Promega | Cat# L1195 |
| Biological Samples | | |
| Human lung adenoma tissue sections | University of Wuerzburg. Institute of Pathology | N/A |
| Mouse lung tissue sections | Gaubatz lab | N/A |
| Chemicals, Peptides, and Recombinant Proteins | | |
| Recombinant human EGF | Sigma | Cat# E9644 |
| Verteporfin | Sigma | Cat# SML0534 |
| Agencourt AMPure XP beads | Beckmann Coulter | Cat# A63882 |
| 4-hydroxytamoxifen | Sigma | Cat# H7907 |
| Doxycycline | Sigma | Cat# D9891 |
| Neomycin | Sigma | Cat# N1876 |

(*Continued on next page*)

*Continued*

| REAGENT or RESOURCE | SOURCE | IDENTIFIER |
|---|---|---|
| Hydrocortisone | Sigma | Cat# H0888 |
| Cholera toxin | Enzo Life Science GmbH | Cat# BML-G117 |
| Bovine pituitary extract | Thermo Fisher Scientific | Cat# 13028014 |
| Insulin | Sigma | Cat# I9278 |
| Dynabeads Protein G | Thermo Fisher Scientific | Cat# 10004D |
| B27 supplement | Thermo Fisher Scientific | Cat# 17504001 |
| Critical Commercial Assays | | |
| NEBNext® Ultra II DNA Library Prep Kit for Illumina | New England Biolabs | Cat# E7645S |
| NEBNext Ultra RNA Library Prep Kit for Illumina | New England Biolabs | Cat# E7530S |
| NEBNext Multiplex Oligos for Illumina (Dual Index Primers Set 1) | New England Biolabs | Cat# E7600 S |
| Duolink *In Situ* PLA Probe Anti-Rabbit PLUS, Affinity purified Donkey anti-Rabbit IgG (H+L) | Sigma-Aldrich | Cat# DUO92002 |
| Duolink *In Situ* PLA Probe Anti-Mouse MINUS, Affinity purified Donkey anti-Mouse IgG (H+L) | Sigma-Aldrich | Cat# DUO92004 |
| Duolink *In Situ* Detection Reagents Red | Sigma-Aldrich | Cat# DUO82008 |
| Duolink *In Situ* Wash Buffers, Fluorescence | Sigma-Aldrich | Cat# DUO92049 |
| NextSeq 500/550 High Output Kit v2 (75 cycles) | Illumina | Cat# FC-404-2005 |
| QIAquick PCR Purification Kit | QIAGEN | Cat# 28106 |
| Phusion Hot Start II DNA Polymerase | Thermo Fisher Scientific | Cat# F549L |
| NEBNext Poly(A) mRNA Magnetic Isolation Module | New England Biolabs | Cat# E7490 |
| Quant-iT PicoGreen dsDNA Assay Kit | Thermo Fisher Scientific | Cat# P11496 |
| RNeasy Mini Kit | QIAGEN | Cat# 79254 |
| Experion DNA 1K Analysis Kit | Bio-Rad | Cat# 7007103 |
| Experion RNA StdSens Analysis Kit | Bio-Rad | Cat# 7007103 |
| High Sensitivity NGS Fragment Analysis Kit | Advanced Analytical | DNF-474 |
| SYBR Select Master Mix | Thermo Fisher Scientific | Cat# 4472908 |
| RevertAid Reverse Transcriptase | Thermo Fisher Scientific | Cat# EP0441 |
| RiboLock RNase Inhibitor | Thermo Fisher Scientific | Cat# EO0384 |
| T4 DNA Ligase | New England Biolabs | Cat# M0202T |
| EcoRI | Thermo Fisher Scientific | Cat# ER0273 |
| HindIII | Thermo Fisher Scientific | Cat# ER0503 |
| HaeIII | New England Biolabs | Cat# R0108T |
| NlaIII | New England Biolabs | Cat# R0125S |
| Deposited Data | | |
| Sequencing data | This study | GEO: GSE115787 |
| Experimental Models: Cell Lines | | |
| KPL-CreER | Iltzsche et al. (2017) | N/A |
| HEK293T | ATCC | Cat# CRL-3216 |
| MCF10A-YAP5SA | von Eyss et al. (2015) | N/A |
| MCF10A-B-MYB | This study | N/A |
| MCF10A-YAP5SA-B-MYB | This study | N/A |
| HeLa | ATCC | Cat# CCL-2 |
| MDA-MB-231 | ATCC | Cat# HTB-26 |
| A549 | ATCC | Cat# CCL-185 |
| Oligonucleotides | | |
| DNA oligonucleotides and siRNA sequences are listed in Table S3 | N/A | N/A |

(*Continued on next page*)

*Continued*

| REAGENT or RESOURCE | SOURCE | IDENTIFIER |
|---|---|---|
| Recombinant DNA | | |
| pINDUCER-20-B-MYB | This article | N/A |
| psPAX.2 | Didier Trono | Addgene Cat# 12260 |
| pCMV-VSV-G | Bob Weinberg | Addgene Cat# 8454 |
| pGL3-promoter | Promega | Cat# E1761 |
| pCMV-2xflag-YAP5SA | Kunliang Guan | Addgene Cat#27371 |
| pCDNA3-HA-TEAD4 | Björn von Eyss | N/A |
| CMV-β-gal | Stefan Gaubatz | N/A |
| pCDNA4/TO-HA-B-MYB | Stefan Gaubatz | N/A |
| pCDNA4/TO HA-B-MYB 1-410 | This article | N/A |
| pCDNA4/TO HA-B-MYB 411-700 | This article | N/A |
| pGEX4T2-YAP-WW1/2 | Stefan Gaubatz | N/A |
| Software and Algorithms | | |
| Bowtie v1.1.2 and v2.3.2 | Langmead et al. (2009), (2012) | N/A |
| MACS v2.2.1. | Zhang et al. (2008) | N/A |
| BEDTools v2.26.0 | Quinlan and Hall (2010) | N/A |
| TopHat v2.1.0 | Kim et al. (2013) | N/A |
| GSEA | Subramanian et al. (2005) | N/A |
| DeepTools | Ramírez et al. (2014) | N/A |
| Prism 7.0 and 8.0 | GraphPad | N/A |
| Integrative genomics viewer | Robinson et al. (2011) | N/A |
| CASAVA | Illumina | N/A |
| FASTQ generation software v1.0.0 | Illumina | N/A |
| edgeR | Robinson et al. (2010) | N/A |
| DAVID v6.8 | Huang et al., 2009 | N/A |
| Sicer v.1.1 | Xu et al., 2014 | N/A |
| 4CSeq analysis pipeline | https://github.com/WGLab/w4CSeq | N/A |
| ROSE | Whyte et al. (2013) | N/A |
| R | https://www.r-project.org | N/A |

## CONTACT FOR REAGENT AND RESOURCE SHARING

Further information and requests for resources and reagents should be directed to and will be fulfilled by the Lead Contact, Stefan Gaubatz (stefan.gaubatz@biozentrum.uni-wuerzburg.de).

## EXPERIMENTAL MODEL AND SUBJECT DETAILS

### Cell lines

KPL-CreER lung adenocarcinoma cells (female) and MCF10A-YAP5SA cells (female) have been described previously (von Eyss et al., 2015; Iltzsche et al., 2017). MCF10A-B-MYB and MCF10A-YAP5SA-B-MYB cells were generated with a lentiviral pINDUCER20-B-MYB expression construct to infect MCF10A and MCF10A-YAP5SA cells, respectively.

KPL-CreER cells were grown in DMEM supplemented with 10% FCS (Thermo Fisher Scientific) and 1% penicillin/streptomycin (Thermo Fisher Scientific). To delete *Lin9*, KPL-CreER cells were treated with 10 nM 4-OHT (Sigma). MCF10A cells were cultured in DMEM/F-12 supplemented with 5% horse serum (Sigma), 1% penicillin/ streptomycin (Thermo Fisher Scientific), 10 μg/ml insulin (Sigma), 500 ng/ml hydrocortisone (Sigma), 20 ng/ml EGF (Sigma) and 100 ng/ml cholera toxin (Enzo Life Science). The expression of YAP5SA was induced in MCF10A-YAP5SA cells by the addition of 0.5 μg/ml doxycycline. MCF10A-YAP5SA cells were synchronized in G0 by culturing in medium without serum and without EGF for 2 days. A549 cells (ATTC #CCL-185, male) were cultured in RPMI (Thermo Fisher Scientific) with 10% FCS and 1% penicillin/ streptomycin. To inhibit the TEAD-YAP interaction, A549 cells were treated with 7.5 μM verteporfin (Sigma) for 24 h. HeLa cells (ATCC #CCL-2, female) and MDA-MB-231 cells (ATTC #HTB-26, female) were cultured in DMEM supplemented with 10% FCS and 1% penicillin/ streptomycin.

## METHOD DETAILS

### Lentiviral production and infection

Lentiviral particles were generated in HEK293T cells cotransfected with psPAX2, pCMV-VSV-G and pINDUCER20-B-MYB. Infected cells were selected 48 h after infection with 300 μg/ml neomycin (Sigma) for 7 days.

### siRNA transfection

Double-stranded RNA was purchased from Eurofins. siRNAs were transfected in a final concentration of 30 nM using RNAiMAX (Thermo Fisher Scientific) according to the manufacturer's protocol. siRNA sequences are listed in Table S3.

### Mammosphere assays

For mammosphere assays, MCF10A cells were seeded in triplicates at a density of 1000 cells/$cm^2$ in 24-well ultra-low attachment plates (Costar) in DMEM/F12 supplemented with 1% penicillin/streptomycin, 52 μg/ml bovine pituitary extract (Thermo Fisher Scientific), 0.5 μg/ml hydrocortisone (Sigma), 5 μg/ml insulin (Sigma), 100 ng/ml EGF (Sigma) and 1x B27 supplement (Thermo Fisher Scientific). To induce the expression of YAP5SA or B-MYB, cells were plated in the presence of 0.5 μg(/ml doxycycline (Sigma). B-MYB was depleted by transfection with the B-MYB specific siRNA 24 h before plating MCF10A-YAP5SA cells. Mammospheres were counted after 7 days.

### RT-qPCR

Total RNA was isolated with peqGOLD TriFast (Peqlab). 2.5 μg RNA was transcribed using 100 units RevertAid reverse transcriptase (Thermo Fisher Scientific). Quantitative real–time PCR reagents were from Thermo Fisher Scientific and real-time PCR was performed using the Mx3000 (Stratagene) detection system. Primer sequences are listed in Table S3. Expression differences were calculated as described before (Osterloh et al., 2007).

### ChIP and ChIP-sequencing

For ChIP, 6.6 × $10^6$ KPL-CreER cells or 1.4 × $10^7$ MCF10A-YAP5SA cells were cross-linked with 1% formaldehyde (Sigma) for 10 min at room temperature. The reaction was stopped by adding 125 mM glycine (Sigma). After cells were lysed for 10 min on ice [5 mM PIPES pH 8.0, 85 mM KCl, 0.5% NP40, 1 mM PMSF, protease inhibitor cocktail (Sigma)], nuclei were resuspended in RIPA buffer [50 mM HEPES pH 7.9, 140 mM NaCl, 1 mM EDTA, 1% Triton X-100, 0.1% sodium deoxycholate, 0.1% SDS, 1 mM PMSF, protease inhibitor cocktail (Sigma)]. Chromatin was fragmented to an approximate length of 150 to 300 bp using a Branson sonifier. Antibodies were bound to protein G-dynabeads (Thermo Fisher Scientific) overnight at 4°C. Beads were washed three times with 5 mg/ml BSA in PBS and incubated with fragmented chromatin for 6 h at 4°C. Beads were washed in total nine times with wash buffer I [20 mM Tris HCl pH 8.1, 150 mM NaCl, 2 mM EDTA, 0.1% SDS, 1% Triton X-100], wash buffer II [20 mM Tris HCl pH 8.1, 500 mM NaCl, 2 mM EDTA, 0.1% SDS, 1% Triton X-100], and wash buffer III [10 mM Tris HCl pH 8.1, 250 mM LiCl, 1 mM EDTA, 1% NP40, 1% sodium deoxycholate]. 1 mM PMSF and protease inhibitor cocktail were added freshly to all buffers. After washing once in 1x TE buffer, chromatin was eluted two times by adding 250 μl freshly prepared elution buffer [1% SDS, 0.1 M $NaHCO_3$] for 15 min at room temperature. To reverse crosslinks the chromatin was incubated with 160 mM NaCl and 20 μg/ml RNaseA at 65°C overnight. Proteins were digested by adding 5 mM EDTA and 200 μg/ml proteinase K at 45°C for 2 h. DNA was purified using the QIAquick PCR Purification Kit (QIAGEN) and eluted in 50 μl EB buffer. Chromatin (1 μl) was used as a template for quantitative real-time PCR. Primer sequences are listed in Table S3.

For ChIP-seq chromatin from 2 × $10^7$ KPL-CreER or 3.5 × $10^7$ MCF10A-YAP5SA cells was isolated and immunoprecipited as described above. Purified ChIP-DNA was quantified using the Quant-iT PicoGreen dsDNA Assay Kit (Thermo Fisher Scientific). Libraries for ChIP-seq were generated using the NEBNext® Ultra II DNA Library Prep Kit for Illumina® (New England Biolabs) according to the manufacturer's instructions. Size-selection was performed using Agencourt AMPure XP beads (Beckman Coulter) (150 bp). DNA fragments were amplified by 10-15 cycles of PCR and library quality was analyzed with the Biorad Experion system and the Fragment Analyzer (Advanced Analytical). The amount of library DNA was quantified using pico green and subjected to Illumina NextSeq 500 sequencing. Base calling was performed with the Genome Analyzer Data Collection Software. The following antibodies were used: B-MYB (Santa Cruz Biotechnology, sc-724), H3K4me1(Abcam, ab8895), H3K4me3 (Abcam, ab8580), H3K27Ac (Merck, 07-360), LIN9 (Bethyl, A300-BL2981), YAP (NB110-58358) and IgG from rabbit serum (Sigma, I5006).

### RNA-seq analysis

RNA was isolated in triplicates from untreated or 4-OHT treated KPL-CreER cells. DNA libraries were generated with 1 μg RNA with the NEBNext Ultra RNA Library Prep Kit for Illumina (New England Biolabs). Library quality was analyzed with the Biorad Experion system. Libraries were sequenced on the NextSeq 500 platform (Illumina).

### Immunoblotting and immunoprecipitation

Cells were lysed in TNN [50 mM Tris (pH 7.5), 120 mM NaCl, 5 mM EDTA, 0.5% NP40, 10 mM $Na_4P_2O_7$, 2 mM $Na_3VO_4$, 100 mM NaF, 1 mM PMSF, 1 mM DTT, 10 mM β-glycerophosphate, protease inhibitor cocktail (Sigma)]. Proteins were separated by SDS-PAGE,

transferred to PVDF membrane and detected by immunoblotting with the following primary and secondary antibodies: β-Actin (Santa Cruz Biotechnology, sc-47778) 1:5000, B-MYB (clone LX015.1, (Tavner et al., 2007)) 1:3-1:5, CDC20 (Santa Cruz Biotechnology, sc-13162) 1:500, Cyclin A (Santa Cruz Biotechnology, sc-239) 1:500, Cyclin B (Santa Cruz Biotechnology, sc-245) 1:1000, anti-FLAG (Sigma, F3165) 1:5000, anti-H2B (Abcam, ab1790) 1:20000 anti-HA (Covance, MMS-101P) 1:1000, LIN9 (Bethyl, A300-BL2981) 1:2000, TOP2A (Santa Cruz Biotechnology, sc-365916) 1:1000, α-Tubulin (Santa Cruz Biotechnology, sc23948) 1:1000, Vinculin (Sigma, V9131) 1:10000, YAP (Santa Cruz Biotechnology, sc-10199) 1:1000, YAP (Cell Signaling, 4912) 1:1000, phospho-YAP (ser127) (Cell Signaling, 4911) 1:1000, anti-mouse HRP conjugated (GE Healthcare, NXA931) 1:5000, HRP Protein A (BD Biosciences, 610438) 1:5000 and mouse TrueBlot ULTRA: Anti-Mouse Ig HRP (Rockland, 18-8817-30) 1:1000.

For immunoprecipitation (IP) of FLAG-tagged proteins, cells were transfected with pCMV-2xflag-YAP and pCDNA-HA-B-MYB. 2 mg lysate was immunoprecipitated with 2.5 μg FLAG-antibody (Sigma, F3165) and collected with protein G dynabeads (Thermo Fischer Scientific). After washes with TNN, proteins were separated by SDS-PAGE and detected by immunoblotting with anti-FLAG (Sigma, F3165) and HA (Covance, MMS-101P) antibodies. For IP of endogenous proteins, nuclear extracts were generated. After cells were lysed [10 mM HEPES pH 7.4, 10 mM NaCl, 3 mM $MgCl_2$, protease inhibitor cocktail (Sigma)] for 20 min on ice, pelleted nuclei were resuspended in nuclei lysis buffer [20 mM HEPES pH 7.4, 400 mM NaCl, 1.5 mM $MgCl_2$, 0.1 mM EDTA, 1% NP40, 15% glycerol, 0.5 mM DTT, protease inhibitor cocktail (Sigma)] for another 20 min on ice. After spinning at full speed for 10 min, the supernatant containing the nuclei was mixed 1:1 with 20 mM HEPES pH 7.4 and used for setting up IPs. 2 μg YAP antibody (Novus, NB110-58358), B-MYB antibody (Santa Cruz Biotechnology, sc-724) or IgG from rabbit serum (Sigma, I5006) coupled to protein G-dynabeads for 1 h were incubated with 2 mg of pre-cleared nuclear extracts for 4 h at 4°C. Beads were washed five times with nuclei lysis buffer mixed 1:1 with 20 mM HEPES pH 7.4. Proteins were eluted from beads and used for SDS-PAGE and immunoblotted.

### GST-pulldown assays

Recombinant GST or GST-WW1/2-YAP (WW domain 1 and 2 of YAP fused to GST) were expressed in BL21 cells and purified on glutathione-linked Sepharose beads (Thermo Fisher Scientific). Lysates of HeLa cells expressing HA-tagged B-MYB constructs were incubated with 5 μg immobilized GST or GST-WW1/2-YAP for 3 h at 4°C. Beads were washed six times with TNN buffer, resuspended in SDS protein sample buffer, boiled for 5 min, separated on a 12.5% SDS-PAGE gel, blotted and analyzed via immunoblotting.

### Subcellular fractionation

For fractionation of nuclear and cytoplasmic proteins, cells were first lysed in in buffer 1 [0.1% NP-40, 137 mM NaCl, 2.7 mM KCl, 10 mM $Na_2HPO_4$ 1.8 mM $KH_2PO_4$, 1 mM PMSF, 1 mM DTT, 10 mM β-glycerophosphate, protease inhibitor cocktail (Sigma)]. After a brief centrifugation the supernatant was removed (cytosolic fraction). The pellet was washed once in buffer 1. Nuclei were lysed in nuclear lysis buffer [ 20 mM HEPES pH 7.4, 400 mM NaCl, 1.5 mM $MgCl_2$, 0.1 mM EDTA, 1% NP-40, 15% glycerol, 0.5 mM DTT, protease inhibitor cocktail] for 15 min on ice and then sonicated in a Biorupter for 5 min with 30 s ON/ OFF cycles. Next the lysate was cleared by centrifugation and the supernatant was transferred to a fresh tube (nuclear fraction)

### Luciferase assays

KIF23 enhancers E1-E4 were amplified by PCR and cloned into the pGL3-promoter vector (Promega). Reporter plasmids were co-transfected with pCMV-2xFlag-YAP-5SA and pCDNA3-HA-TEAD4 expression plasmids into HEK293T cells in a 24-well format. Cells were lysed in passive lysis buffer (Promega) for 10 min. Luciferase activity was measured with firefly buffer [22.5 mM glycyl-glycine, 10 mM $MgSO_4$, 2 mM ATP, 18 μM luciferin]. To normalize for transfection efficiency, 160 ng of CMV-β-gal was cotransfected and β-gal activity was determined.

### PLA

PLA was performed using the Duolink *In Situ* Kit (Sigma) according to the manufacturer's instructions. The following antibodies were used: LIN9 (Bethyl, A300-BL2981; 1:150), B-MYB phospho-T487 (ab76009; 1:100), YAP (Santa Cruz Biotechnology, sc-101199; 1:200). Pictures were taken with an inverted Leica DMI 6000B microscope equipped with a Prior Lumen 200 fluorescence light source and a Leica DFC350 FX digital camera.

### Circular Chromosome Conformation Capture assays (4C-seq)

4C-seq was performed as described previously with some modifications (Stadhouders et al., 2013). MCF10A-YAP5SA cells were incubated for 10 min at room temperature with 1.5% formaldehyde in PBS followed by 5 min treatment with 0.125 M glycine in PBS. Cells were collected with a cell scraper, washed in PBS and lysed in 3 mL lysis buffer [50 mM Tris-HCl, pH 7.5, 150 mM NaCl, 5 mM EDTA, 0.5% NP40, 1% Triton X-100, protease inhibitor cocktail] by one freeze /thaw cycle (1 h at −20°C, 1 h thawing on ice) and by passing 20 times through a syringe attached to a 20 gauge needle. Nuclei were collected at 1200 rpm for 5 min and washed with 1.2x restriction buffer (EcoRI buffer or R buffer, Thermo Fisher Scientific). Nuclei were resuspended in 0.5 mL 1.2x restriction buffer and treated with 0.3% SDS at 37 °C for one h. Triton X-100 was added to a final concentration of 2% and incubated at 37°C for 1 h. HindIII or EcoRI (both from Thermo Fisher Scientific) digestion was performed with 400 U of enzyme at 37 °C overnight.

After de-crosslinking with 1.6% SDS for 20 min at 65°C, the sample was diluted with 6.125 mL of 1.15 x ligation buffer (New England Biolabs) and Triton X-100 was added to a final concentration of 1%. Proximity ligation was performed with 8000 units T4 DNA Ligase (New England Biolabs) at 4 °C for 16 hours. After reversing the cross-linking with 300 μg proteinase K at 65°C overnight and incubating with 300 μg RNase A for 30 min at 37°C, the DNA was purified using a phenol-chloroform extraction and precipitated with ethanol. 50 μg of the 3C library was digested with 50 units NlaIII or HaeIII (both from New England Biolabs) overnight at 37°C. The DNA was purified by phenol-chloroform extraction, precipitated with ethanol and ligated with 16,000 units T4 DNA ligase (New England Biolabs) at 16°C overnight. After a phenol/chloroform extraction, the DNA was ethanol precipitated and purified using the QIAquick PCR Purification Kit (QIAGEN). Next, PCR reactions with Phusion Hot Start II DNA Polymerase (Thermo Scientific Scientific) and with primers containing P5/P7 Illumina adaptors were performed. After the PCR reaction, the 4C library was purified using the QIAquick PCR Purification Kit (QIAGEN) and Agencourt AMPure XP beads (Beckman Coulter). The libraries were sequenced using an Illumina NextSeq 500 sequencer. The following combinations of primary and secondary restriction enzymes were used: Cdc20: EcoRI, NlaIII; Aurka: HindIII, NlaIII; Mybl2: HindIII, NlaIII; Kif23: HindIII, HaeIII.

### Immunostaining and immunohistochemistry

For immunostaining, cells were plated onto coverslips in 30 mm cell culture dishes and fixed in 3% paraformaldehyde and 2% sucrose in PBS for 10 min at room temperature. Cells were permeabilized with 0.2% Triton X-100 in PBS for 5 min, blocked in 5% BSA in PBS-T (0.1% Tween 20) and incubated with primary antibody diluted in 1% BSA in PBS-T at room temperature for 1 h. The following antibodies were used: phospho-Histone H3 (Ser10) (Santa Cruz Biotechnology, sc-8656) 1:100, α-Tubulin (Santa Cruz Biotechnology, sc-23948) 1:150, YAP (Cell Signaling, 14074) 1:200. After washing several times in PBS-T, coverslips were incubated with secondary antibody conjugated to Alexa Fluor 488 or 594 (Thermo Fisher Scientific) and Hoechst 33258 (Sigma) both diluted 1:500 in 1% BSA in PBS-T at RT for 30 min. Mouse lung tissue sections were deparaffinized, rehydrated, and processed for immunohistochemistry staining. For immunohistochemistry, sections were incubated for 10 min with 3% $H_2O_2$ to quench endogenous peroxidase. Antigen retrieval was performed in 10 mM sodium citrate buffer (pH 6.0) by boiling in a microwave for 6 min. Slides were blocked with 3% BSA in PBS-T (0.1% Tween 20) and incubated with primary antibodies (B-MYB phospho T487 (Abcam, ab-76009) 1:400 and YAP (Cell Signaling, 4912) 1:200) diluted in blocking solution overnight at 4°C. Secondary antibody (anti-rabbit HRP conjugated; Thermo Fisher Scientific), was applied to sections at 1:200, incubated for 1–2 h at room temperature and developed in diaminobenzidine. Human adenocarcinomas of the lung were stained immunohistochemically following antigen retrieval with pressure cooking (citric acid pH 6.0).

### Gene set enrichment analysis (GSEA)

GSEA (Broad Institute) was performed as described previously (Subramanian et al., 2005) with 1000 permutations, "Signal2Noise" metric of RNA-seq read counts per gene and a gene set size filter of 15-900. The "C2" gene set database from MSigDB was spiked with YAP signatures from MSigDB "C6" ("Cordenonsi: YAP conserved signature") as well as "YAP/TAZ" (Zhang et al., 2009), "induced by YAP" (Zhao et al., 2008), "YAP" (Dupont et al., 2011) and "YAP signature" (Zanconato et al., 2015).

To stratify tumors from normal tissue or late-stage from early-stage tumors two gene sets reflecting YAP-direct targets (defines as genes with a YAP peak in ± 0.5 kb around the TSS) and MMB-YAP targets (defined by YAP-bound enhancers that loop to a LIN9-bound promoter) were defined. Normalized gene expression data were downloaded from TCGA or GEO (GSE18842, GSE3398, GSE16476, GSE20916), samples were divided into "normal," "tumor," "stage 4" or "low stage" as indicated and the GSEA algorithm was used with default settings to examine gene expression of direct YAP targets and MMB-YAP target genes.

### Bioinformatics

Base calling was performed with Illumina's CASAVA software or FASTQ Generation software v1.0.0 and overall sequencing quality was tested using the FastQC script. For ChIP-sequencing, reads were mapped to the human (hg19) or murine (mm10) genome with Bowtie v1.1.2 (Langmead et al., 2009) with default parameters. Mapped reads were randomly subsampled to the sample with the smallest number of mapped reads and peak calling for transcription factors was performed with MACS v2.1.1 (Zhang et al., 2008) and corresponding input samples as controls with variable "–keep-dup" settings (3 for Yap/YAP, 5 for Lin9/LIN9/B-MYB) and q-value cut-off (5.0e-2 for Yap/Lin9, 1.0e-3 for LIN9/B-MYB, 1.0e-5 for YAP). Enrichments for histone modifications were determined using SICER v1.1 (Xu et al., 2014) with a window size of 200 bp, gap size of 600 bp and a q-value cut-off of 1.0e-3. Enhancer are defined by having an enrichment for H3K4me1 overlapping with H3K27ac without H3K4me3 enrichment and being at least 1 kb away from annotated TSS of Ensembl genes (mouse: GRCm38.p6, human: GRCh37.p13). Open and active promoters are defined by having an enrichment for H3K4me3 overlapping with H3K27ac without H3K4me1 enrichment and being in a region of ± 1 kb around annotated TSS of Ensembl genes. H3K27ac enrichments and read density were used to identify super-enhancers with the ROSE software (Whyte et al., 2013). For visualization, read density files in bedgraph format were generated using the *genomeCoverageBed* function from bedTools v2.26.0 (Quinlan and Hall, 2010) and the Integrated Genome Viewer (Robinson et al., 2011). Heatmaps and density profiles were generated using Deeptools (Ramírez et al., 2014) and a resolution between 10 and 100 bp as indicated. The overlap of Lin9 and Yap binding sites was calculated with bedTools intersectBed and at least 1bp overlap and the proportional Venn diagram was drawn with the R package eulerr.

To correlate LIN9 binding with gene expression changes, reads were counted in a region ± 1kb around TSSs of expressed genes with more reads in the LIN9 sample then in input controls (n = 10,981). Genes were sorted based on $log_2$FC (+OHT versus –OHT), grouped into 18 equally sized bins and the mean of all bins was plotted. *P*-values for Pearson's correlation coefficients were calculated with two-tailed t tests.

B-MYB occupancy was analyzed in a region of −100 to +400 bp around TSS and the empirical cumulative distribution function was calculated using the R environment (https://www.r-project.org).

For the analysis of promoter-enhancer interactions, published Hi-C data from IMR90 cells were used (Jin et al., 2013). Positions of "anchor" (TSS) and "target" (enhancer) regions were converted to hg19 coordinates and overlapping "target" regions with YAP (+dox) peaks were identified. For each of these YAP-bound "targets" the corresponding "anchor" was analyzed whether it is overlapping with LIN9 (-dox) peaks, B-MYB is bound and how gene expression changes upon induction of YAP5SA.

Functional analyses of gene groups were done with DAVID v6.8 (Huang et al., 2009) using only gene ontology (GO) terms as database and functional clustering of enriched GO terms.

In boxplots, the median is indicated, borders of boxes show the upper and lower quartile and whiskers extend to 1.5 of the interquartile range.

For RNA-sequencing, read were mapped to *Mus musculus* reference genome mm10 or the *Homo sapiens* genome hg19 using TopHat v2.1.0 (Kim et al., 2013) with Bowtie v2.3.2 (Langmead and Salzberg, 2012) and randomly subsampled based on the sample with the smallest number of mapped reads. Weakly and non-expressed genes were removed (mean read count over all samples < 1) and edgeR (Robinson et al., 2010) was used to identify differentially expressed genes.

The Zanconato et al. YAP target gene signature was analyzed with respect to binding of DREAM and MMB subunits using the TargetGeneReg database (Fischer et al., 2016). The resulting heatmap was row-wise hierarchically clustered using euclidean distance measurements and complete linkage.

Identification of *MYBL2* co-expressed genes in human NSCLC (Sanchez-Palencia et al., 2011) was done by obtaining RMA-normalized signal intensities from GEO, aggregating multiple probes per gene by the maximum and calculation of the Pearsons correlation coefficients for each gene with *MYBL2* expression.

Kaplan-Meier survival curves were calculated with the survfit function from the R package {survival} and corresponding p values were calculated using a logrank test.

For 4C-seq analyses, the reads were trimmed to remove the first 3 base pairs containing the treatment-specific barcode. The publicly available 4CSeq analysis pipeline (https://github.com/WGLab/w4CSeq) was subsequently used with default settings.

Distal regions with an adjusted *P*-value < 0.01 were considered to significantly interact with the viewpoints.

## QUANTIFICATION AND STATISTICAL ANALYSIS

Statistical analyses were performed using Prism 7 and Prism 8 (GraphPad). Tests used to determine statistical significance are indicated in the figure legends. Comparison of two groups was done by a two-sided Student's t test or for more than two groups by one-way analysis of variance (ANOVA) with Tukey's post test. Two-way ANOVA with Bonferroni's multiple comparison test was used for the comparison of two groups in response to two different variables. *P*-values < 0.05 were considered statistically significant. * $p < 0.05$;** $p < 0.01$; *** $p < 0.001$; **** $p < 0.0001$.

## DATA AND SOFTWARE AVAILABILITY

ChIP- and RNA-sequencing datasets are available at the NCBI's Gene Expression Omnibus (Edgar et al., 2002) under the accession number GEO: GSE115787